nature reviews earth & environment

https://doi.org/10.1038/s43017-025-00682-x

Review article

Check for updates

Crystal mush processes and crustal magmatism

Madeleine C. S. Humphreys[1] ✉, Olivier Namur[2] ✉, Wendy A. Bohrson[3], Pierre Bouilhol[4], George F. Cooper[5], Kari M. Cooper[6], Christian Huber[7], C. Johan Lissenberg[5], Eduardo Morgado[8] & Frank J. Spera[9]

Abstract

Much of Earth's magma is stored as extensive crystal mush systems, yet the prevalence of physical processes operating within mushes and their importance in volcanically active regions remain enigmatic. In this Review, we explore the physical properties and key processes of crystal mush systems. The initiation, evolution and decline of volcanic systems, modulated by heat supply and loss, could generate differences in the prevalence of mush processes through space and time. Additionally, regional tectonics alter mush properties, with mushes in cool wet settings having persistent residual melt, permitting more effective melt segregation than in hot dry settings. Disaggregation of mushes results in crystal mush material being mobilized or entrained into lavas and erupted, presenting opportunities to define the timescales and chemistry of some mush processes in volcanically active regions. Mush systems can be observed on length scales ranging from kilometres (using geological mapping) to micrometres (using crystal textures). Therefore, it is difficult to integrate data and interpretations across different fields. Improved integration of thermodynamics, textural analysis, geochemistry, modelling and experiments, alongside inputs from adjacent fields such as porous media dynamics, engineering and metallurgy will help to advance understanding of mush systems and ultimately improve hazard evaluation at active and dormant volcanic systems.

Sections

[1]Department of Earth Sciences, Durham University, Durham, UK. [2]Department of Earth and Environmental Sciences, KU Leuven, Leuven, Belgium. [3]Department of Geology and Geological Engineering, Colorado School of Mines, Golden, CO, USA. [4]Université de Lorraine, CNRS, CRPG, Nancy, France. [5]School of Earth and Environmental Sciences, Cardiff University, Cardiff, UK. [6]Department of Earth and Planetary Sciences, University of California Davis, Davis, CA, USA. [7]Department of Earth, Environmental and Planetary Sciences, Brown University, Providence, RI, USA. [8]Escuela de Geología, Universidad Mayor, Santiago, Chile. [9]Department of Earth Science, University of California, Santa Barbara, CA, USA. ✉e-mail: madeleine.humphreys@durham.ac.uk; olivier.namur@kuleuven.be

Key points

- All magmas transition through a mush stage during solidification, when there is an interconnected solid framework that can transmit stress with an interconnected liquid in the pore spaces.
- Long-lived crystal mushes are the site for the enrichment, segregation and deposition of many mineral deposits and are important for productive geothermal systems. Additionally, mush instability is closely linked to volcanic eruption.
- The physical behaviour of mushes depends primarily on porosity, melt viscosity, permeability, and crystal shape and size distribution. These properties can vary substantially across different length scales.
- Cumulates represent the crystalline residue left over after the segregation of crystals or the extraction or migration of silicate melt during igneous differentiation. Cumulates are complementary to erupted magmas.
- Melt migration in crystal mushes can occur by grain-scale porous flow or channelization. Reactive melt migration can affect crystal mush porosity, permeability and composition, and therefore alter the chemical evolution of the residual liquid.
- The thermal maturation of volcanic systems enhances crystal–melt segregation in the crust and is expected to increase the migration, reaction and extraction of melt from mush. Disaggregation of mush can transfer crystal cargo to erupting magmas.

Introduction

Volcanic systems are the outward expression of plate tectonics and heat loss from the Earth, producing magma storage reservoirs and transport pathways that contain crystal mush: regions of molten rock containing a crystal framework and varying amounts of melt and fluid[1] (Fig. 1). Geophysical information (such as seismic velocity, tomography, gravity or magnetic data) indicate that the quantity of silicate melt within the crust is relatively small (≤15% (refs. 2–4)). These observations suggest that melt-rich bodies are ephemeral[5] and instead magma is mostly stored as crystal mush. Crystal mush processes (such as solidification, melting, and physical separation of crystals and silicate melt) govern igneous differentiation in all geological scenarios where partial melt is present, including deep mountain-building environments, subduction systems, mid-ocean ridges and ocean islands.

Mush and magma form part of a continuum from fully liquid to fully solid. Crystal mush can be defined as a super-solidus rock with a largely interconnected melt phase[5–8] within a continuous crystal framework[8,9] and with variable fluid content (Fig. 1). The chemical and physical properties of a crystal mush (such as temperature, melt composition, density, tensile strength and seismic velocity) change dramatically with crystal fraction[1] (Fig. 1). The overall rheology of crystal mush is controlled by the properties of the solid crystal framework[5,8,9]. In contrast, magma can be defined as a melt with solid crystals and varying amounts of fluid in suspension, with a rheology that is largely controlled by the continuous melt phase[8–10]. Mushy rocks can form through magma crystallization or through the partial melting of the crust caused by regional or contact metamorphism[9], and the definition of crystal mush can be applied equally to crystallization or partial melting[9,11]. This Review primarily focuses on crystallization, but we do not intend to imply a one-directional process. Long-lived mush systems can undergo many iterations of crystallization, resorption and recrystallization[12,13], and partial melting of the crust can be a crucial part of magma generation and differentiation[9,11].

Mushes provide insight into multistage crustal magmatic processes that cannot be determined from melts alone. For example, the prevalence of crystal mush is an indicator of the heat and mass balance from the mantle to the crust. Interpreting geophysical data to image magma storage and transport zones requires knowledge of crystal mush properties. Understanding of crystal mush processes can give insights into the timescales and mechanisms of system change in the lead up to eruptions, and therefore represents a route towards the anticipation of future eruptions.

In this Review, we examine mush processes in crustal magmatic systems across space and time as related to tectonic setting, the evolution of volcanic systems and the precursors to volcanic eruptions. First, we discuss the different strands of evidence that are used to constrain the occurrence of mush, and summarize the physical and chemical processes that operate during mush formation, rejuvenation and eruption. We then evaluate the relative importance of these processes in the context of the evolving thermal maturity of volcanic systems and across different tectonic settings. We discuss how pre-eruptive mush processes link to the timescales obtained by radiometric dating or diffusion chronometry of erupted crystals. We conclude that advances in understanding mushes are likely to arise by improving the integration of evidence from petrology, geochemistry, geophysics, analogue experiments and dynamical numerical models, across diverse spatial scales.

Evidence and importance of crystal mushes

Understanding how materials are formed and processed through crystal mushes provides insight on geodynamics, rates of magma transport, the extraction of partial melts from their source, and timescales of volcanism and crust formation. Cooling magma spends most of its lifetime as mush[14]; therefore, the timescales of magma generation and extraction are intrinsically linked to the physics and rheology of multiphase systems. Mush processes are also important for natural resources; for example, active convection of melt within mushes is partly responsible for the high rate of heat transport required for efficient geothermal systems[15]. Additionally, changes in melt chemistry during igneous differentiation generate the chemical enrichment required for the formation of various mineral resources, including deposits of chromite[16], rare earth elements[17], platinum group elements[18] and copper[19]. Finally, the presence of silicate melt influences the bulk strength, elastic properties and strain partitioning behaviour of the crust. Therefore, multiparametric geophysical evidence[20] and numerical modelling of crustal thermal structure[21] provide strong evidence for the presence of melt within the crust. Understanding the formation, behaviour and solidification of mush is key to linking real-time surface geophysical observations to subsurface magmatic processes[22].

All magma bodies equilibrate thermally with the crust and solidify by progressive crystallization, passing through a mushy state. Samples of mush can be disrupted and brought to the surface by eruptions across all tectonic settings, from arc volcanoes[23] to mid ocean ridges[24], providing snapshots of crystal mush solidification. These samples include melt-bearing nodules[25–27], plutonic enclaves[28–30], and crystal clots and glomerocrysts[31], as well as plutonic rocks exposed at the Earth's surface. In these samples, grain-scale textures and geochemistry

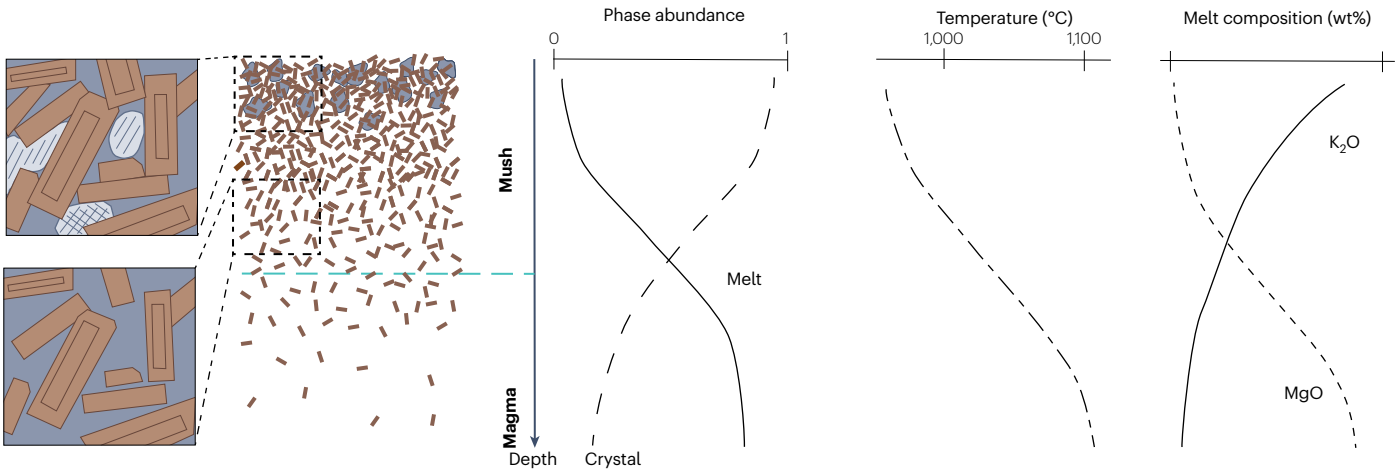

Fig. 1 | Schematic mush cross-section. Left: the distribution of crystals within a mush as a function of depth. The insets show illustrative mush textures with tabular primocrysts (brown); a space-filling, interstitial phase (pale grey); and melt (darker grey). The horizontal dashed blue line schematically indicates the transition from magma to mush. Right: the phase abundances (melt fraction, solid line; crystal fraction, dashed line); temperature; and melt composition (K_2O, incompatible, solid line; MgO, compatible, dashed line) of a cooling intrusion. These schematics are based on direct observations of crystal mush sampled by drilling in Makaopuhi lava lake[33] but are not intended to be prescriptive of a particular system. The depth scale is also schematic and could span a few tens of metres from top to bottom, but more broadly is determined by the melt composition and heat balance across the mush. The chemical and physical properties of a crystal mush can change dramatically with depth.

can be used to define crystallization processes, estimate crystal fractions and infer the occurrence of melt convection and compaction or disaggregation of the crystal mush. For example, narrow films of interstitial phases indicate the final locations of crystallization, the formation of replacive grain-boundary textures indicate the occurrence of a localized reaction with migrating late-stage liquids[32], and disequilibrium hornblende overgrowth on clinopyroxene primocrysts is evidence of reactive melt percolation by evolved hydrous melts within the mush[30].

Drilling programmes have been used to sample mushes directly. For example, samples obtained from drilling in lava lakes[33] and during exploration for geothermal resources[15] have revealed progressive changes in crystal content, melt chemistry, mineralogy and physical properties with depth (Fig. 1). These changes are reproduced by laboratory experiments seeking to generate mush by holding samples of basalt at super-solidus temperatures in a thermal gradient[34].

However, the small length scale of these direct sampling approaches cannot provide evidence for larger-scale dynamic mush processes such as differentiation, sedimentation, localized deformation or melt extraction. Instead, evidence for these processes can be found in meso-scale plutonic rock fabrics[9] and bulk rock and mineral chemistry, including individual intrusions as well as exhumed sections of arc or ocean crust. For example, in the Searchlight Pluton, Nevada, large-scale mapping, geochemistry and high-precision geochronology provide evidence for the differentiation and extraction of evolved residual liquid from crystal mush to feed overlying leucogranite sills and volcanic eruptions[35]. Additionally, features of localized high-temperature deformation such as mush faulting and slumping are preserved in steep mushy sidewalls found in the Skaergaard intrusion[36] and in the Sierra Nevada[37].

Crystal mushes and cumulate formation

Cumulates are the crystalline residue left over after the differential movement or segregation of crystals and extraction or migration of silicate melt during igneous differentiation. Mineralogically and chemically, cumulates do not represent a bulk melt or magma composition because the solid phase is over-represented relative to the liquid[38]. Cumulates represent a record of geochemical differentiation that is complementary to erupted magmas and is present in exposed plutons, ophiolites, deep crustal transects and as enclaves in volcanic eruptions[29,39,40]. In this section, we summarize some of the general mechanisms for the formation of cumulate mushes and their signatures in natural rocks, before reviewing the geochemical and physical consequences of these processes.

Crystal settling

Crystals can be separated from liquid by settling. For a single crystal, settling is determined by the crystal size, the density contrast between the solid and the melt, and on the viscous drag between the melt and crystal, which depends on the melt composition and crystal shape[41] and orientation. However, for abundant crystals, crystal–crystal interactions become important and often slow down crystal migration[42–44]. These complex interactions affect the meso-scale properties of crystal mushes such as size distribution and phase abundance[45], and are implicated in the formation of some metal-rich ore horizons[46]. For example, during the settling of dense suspensions, crystal–crystal interactions can lead to the generation of layers defined by crystal size and density[45,47,48], internally differentiating mush packets linked to ore mineralization[18], and density instabilities that result in crystal-laden plumes[44,49,50].

Consolidation of the crystal mush

A loosely packed mush is not at its maximum packing density; melt can therefore be segregated if crystals are consolidated (repacked) into a more efficient spatial arrangement (this process is also known as 'mechanical compaction'[51–53]) by being translated and rotated under gravity or during shear deformation (Fig. 2a,b). In a loosely packed

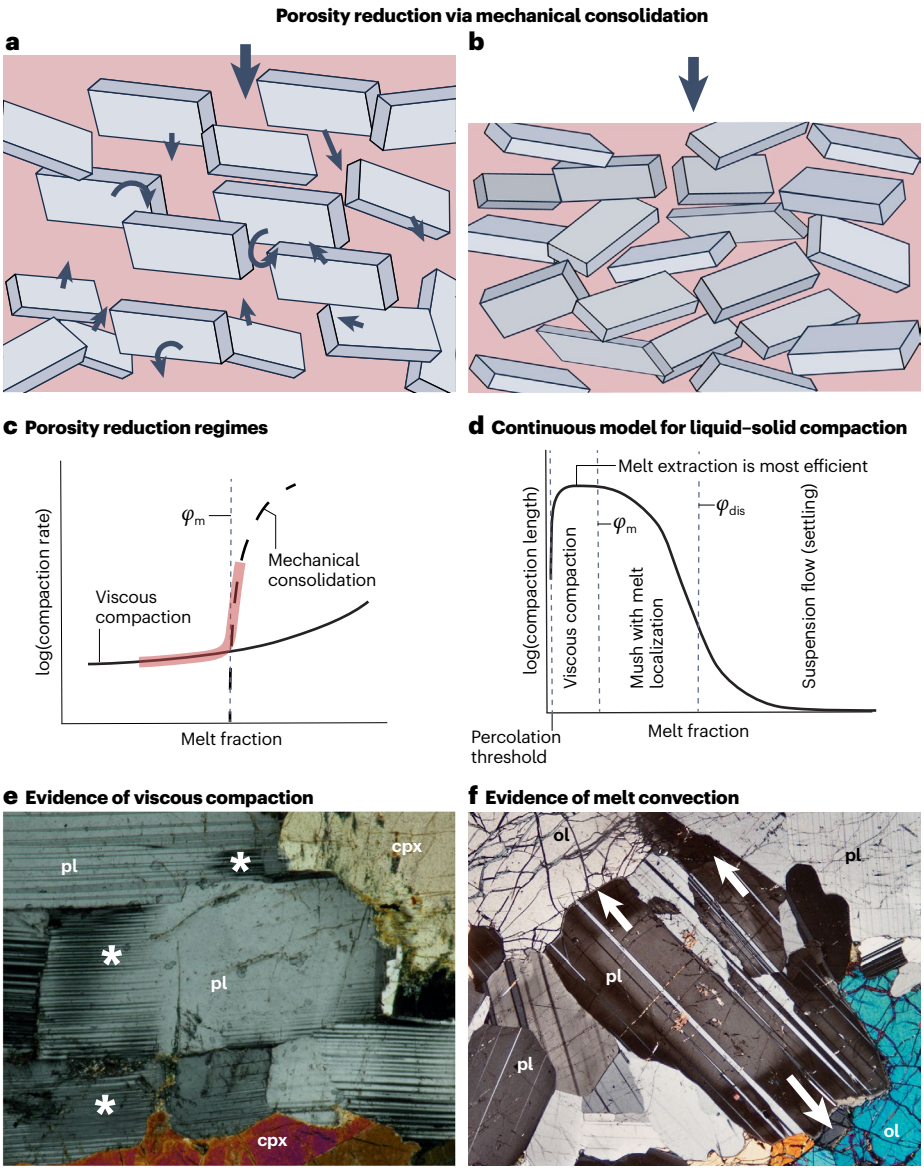

Fig. 2 | Mush compaction. a,**b**, The translation and rotation (thin black arrows) of individual crystals within an initially loosely packed mush (**a**) leads to compaction and porosity reduction of the mush through mechanical consolidation (**b**) in response to applied stress (thick black arrows). When the mush contains anisotropic crystals, this consolidation results in shape-preferred alignment, as shown. **c**, A schematic representation of composite mush rheology[53] (orange line) including contributions from mechanical consolidation (dashed line) and viscous compaction (solid line). The vertical dotted line indicates the melt fraction at the maximum packing fraction, ϕ_m. Compaction occurs primarily by mechanical consolidation at melt fractions $>\phi_m$ and by viscous compaction at melt fractions $<\phi_m$. **d**, Continuous model for liquid–solid compaction length for two-phase flow from porous flow regime (accommodated by viscous compaction at melt fractions $<\phi_m$ and by melt localization between ϕ_m and ϕ_{dis}, the porosity at which mush disaggregates) to suspension flow[49] (crystal settling). **e**, A cross-polarized photomicrograph showing deformation twinning and mechanical bending (asterisks), which provides textural evidence of viscous compaction. **f**, A cross-polarized photomicrograph showing constant composition rim growth (arrows), which provides textural evidence of melt convection. The mush compaction rate changes with crystal fraction and occurs through different mechanisms, some of which might leave a textural trace. cpx, clinopyroxene; ol, olivine; pl, plagioclase. Part **f** adapted from ref. 74, Springer Nature Limited.

mush, melt segregation is dominated by frictional interactions between crystals[54]. These interactions can lead to the formation of force chains between neighbour crystals that localize stress accumulations and deformation within the mush[55]. High-temperature and analogue experiments[46,56,57], and field and petrological research on melt loss in shallow to mid-crustal intrusions[58], suggest that mechanical consolidation can reduce porosity by up to tens of per cent (Box 1). However, this process is limited to mushes with crystal fractions ≤0.7 (ref. 53). Mechanical consolidation is hard to discern in nature because it leaves little textural signature, except for the development of a foliation[59] (Fig. 2b). The strength of this foliation depends on the crystal shape and the extent of melt loss (for example, as estimated by trace-element mass balance[39,53,60,61]). Once the maximum packing density has been reached, the remaining melt can only be expelled by viscous compaction[53] (Fig. 2c,d).

Viscous compaction of the crystal mush

In densely packed mushes, further melt extraction occurs by viscous deformation of the crystal framework, through diffusive pressure solution (that is, dissolution–reprecipitation) processes and by grain boundary diffusion creep[53,62,63]. These processes can be driven by the applied stress, which is related to the density contrast between the melt and crystal phases[63–66]. Resistance to viscous compaction is dominated by viscous drag between the expelled melt and the crystal framework, and also by the high effective viscosity of the matrix[64,65]. Viscous compaction is facilitated by extraction of melt through an interconnected network of melt between the mush framework[67], which develops during progressive textural equilibration between crystals and melt[62,63,68] (Box 1).

The compaction length scale describes the characteristic thickness of the deforming mush layer[49,64,65] (Fig. 2d). This length scale

is expected to range from metres to hundreds of metres, depending on the physical properties of the melt, which are determined by its composition, and the specific processes controlling mush compaction[49,65,69]. When the mush is highly permeable and/or the viscosity of the crystal framework is high, the compaction length can be large compared with the thickness of the mush layer and, in that scenario, compaction is limited only by the deformation rate of the crystal framework[64]. This scenario is valid for thin mushes (with a thickness ranging from one metre to tens of metres, depending on the melt fraction and melt composition). In contrast, in thick mushes (hundreds or thousands of metres thick) the compaction length is substantially smaller than the mush layer thickness and compaction is controlled by both the deformation of the crystal framework and the mush permeability[64,65,69]. In general, compaction should therefore progress more quickly in long-lived, thick mushes with a large density contrast between crystals and melt, than in thin mushes with a small density contrast.

Whether melt can be segregated from a mush by repacking or involves grain boundary diffusion processes, depends on the rate of compaction relative to crystallization (Fig. 2c) because crystallization fills interstitial pore spaces, which progressively inhibits compaction (Fig. 2d). Experiments and mid-crustal to upper-crustal silicic intrusions exhibit a preserved melt fraction that corresponds roughly to their expected maximum crystal packing, suggesting that consolidation (repacking) controls melt loss in these systems[53,70]. This inference is consistent with an experimental observation that viscous deformation has a compaction rate three to five orders of magnitude lower than that of consolidation[53,57]. The rates, mechanisms and textural signatures of viscous deformation and mechanical consolation merit further research because they represent the early stages in the extraction of a potentially eruptible melt that can feed surface volcanic activity, and because they affect the formation of economic resources such as chromitites[46].

Viscous compaction might be identifiable through textural signatures such as undulose extinction, low-angle grain boundaries and mechanical twins[29,71] (Fig. 2e). These signatures arise from free dislocations that form in response to stress. Diffusion-driven pressure solution is expected to result in truncation of grains, formation of sutured or lobate grain contacts, and compositionally distinct overgrowths on favourably oriented crystal faces[29,71–73]. Deformation textures are relatively common in large plagioclase-rich or olivine-rich cumulate bodies[74–76] and can be shown to have formed when melt remained present[71,73]. Evidence of deformation occurring when melt was present is also found in smaller, lower crustal and oceanic gabbros[75,77]. However, there remains disagreement over whether these features are unambiguously linked to compaction driven by the overlying crystal mush or to external tectonic drivers[71,75,78].

Melt convective migration within the mush

Crystal settling, mechanical consolidation and viscous compaction are all processes that act on the mush framework; however, the chemistry and differentiation of the mush system can also be affected by processes

Box 1 | Physical properties of crystal mushes

Porosity and crystal content

Solids in crystal mushes form an interconnected framework through which melt can percolate until the percolation threshold is reached. The crystal fraction above which a magma becomes a mush (Fig. 1) depends on many factors including crystal size and shape (that is, aspect ratio). Structural analysis of natural crystal mush frameworks suggests that the initial crystal fraction can be as low as 0.2 (ref. 208). This finding is consistent with high-temperature basalt partial melting experiments in which rock strength is maintained by chains of interconnected plagioclase crystals, until the crystal fraction is around 0.3 (ref. 209). Analogue experiments to create random, loosely packed mushes show that solid fraction decreases with increasing friction and particle aspect ratio[55,210]. Numerically simulated mushes of anisotropic cuboids (approximating plagioclase shapes) can also have very low solid fraction (<0.2), depending on crystal shape[59,211]. Therefore, the crystal fraction of a natural crystal mush can be locally heterogeneous and increases as the variability of the crystal size increases[212,213]. These characteristics mean that, although crystal mush behaviour is commonly described relative to a rheologically locked state, there is no fixed crystal fraction at which this state occurs because it strongly depends on crystal shape and size distribution.

Permeability

Interstitial liquid can move through the connected pore space of a crystal mush. The rate of melt flow depends on the pressure gradient that drives it (which can arise from buoyancy or external stresses), the melt viscosity and the geometry of the pore space. These characteristics are captured by the permeability, which is typically described using Darcy's law. Flow velocity increases with decreasing melt viscosity, increased pressure gradient and increased permeability[214]. For a mush of spherical particles, the permeability is controlled by the crystal fraction and grain size[69,214,215]. This concept can be generalized to mushes with a substantial size distribution or varied shapes[216–219] by instead considering the specific surface areas of the crystal framework[219,220]. Importantly, the permeability of natural crystal mushes will also be anisotropic (Fig. 2a) if there is a crystal fabric, substantial modal layering or active deformation[117,216,221].

Crystal shape and textural equilibration

Crystals growing freely from a melt at low undercooling typically have a compact, euhedral crystal shape. However, the euhedral growth shape is not texturally equilibrated with adjacent crystals in a mush, or with the interstitial melt[26,67,222]. Textural equilibration (sometimes described as maturation) in the presence of melt creates smoothly curving melt films on two- and three-grain boundaries[32,68,188] and eventually leads to the formation of equilibrium solid–melt dihedral angles[26,51]. The textural equilibration process is largely diffusive[223] and therefore depends on mush temperature and the composition of melt and crystals. Prolonged storage of crystal mush allows textural equilibration to progress through coarsening and diffusive readjustment of crystal boundaries. Textural equilibration can modify the texture and physical properties of the mush, particularly the permeability and percolation threshold[68].

operating on the melt, including convective circulation. Convection is driven by changes in buoyancy arising from chemical or thermal perturbations. In most magmatic systems, melts are less dense than their surrounding crystal framework and evolve towards even lower melt densities as a result of compositional changes. The buoyant interstitial melt can therefore be continuously expelled from the crystal mush through convective separation, and replaced in the pore space by circulating melt from the resident magma body[79,80]. This process, known as compositional convection, enables the interstitial melt to maintain a constant composition[79,81]. The textural signature of compositional convection in cumulates includes crystal overgrowth rims of constant composition[74] (Fig. 2f), mesoscopic pipe structures, which might represent convective return flow[80,82], and adcumulate rocks[74,83].

Convection of interstitial melt within the mush depends on factors such as the contrast in density between phases within the mush, the permeability and thickness of the mush, and the melt viscosity[79], as described by the Rayleigh number. Interstitial melt convection occurs when the Rayleigh number exceeds a critical value (approximately 25–80 (refs. 80,84)). Overall, compositional convection within a crystal mush requires a mush with a thickness of hundreds of metres[80] and relatively high permeability, even for hydrous melts with relatively lower viscosity[82].

Volatile migration and filter pressing

In addition to convective melt migration, volatiles such as H_2O or CO_2 can also percolate within the mush pore spaces. The behaviour of volatiles in a crystal mush is important because they impact the buoyancy of the mush and can carry substantial quantities of metals[85]. As the mush solidifies, volatile exsolution is increasingly favoured because volatiles are typically incompatible and their concentration in the melt therefore increases with melt differentiation. Volatile exsolution (that is, bubble nucleation) is therefore most likely near the top (lower pressure) or in the more evolved parts of mush systems[86].

The nucleation and growth of bubbles within the mush creates a volume change that acts as a pressure source and has been proposed as an efficient means to expel melt; this process is known as gas filter pressing[87–89]. The large positive buoyancy of exsolved magmatic volatiles allows them to migrate through crystal mushes[90,91]. The efficiency of volatile movement through the mush increases with increasing crystal fraction[90,91] and with the ratio of bubble size to crystal size[88,92]. Volatile exsolution and migration is expected to be more important in systems with abundant volatiles. However, volatile transport mostly occurs in the form of viscous fingers[93,94], which limits the amount of melt that can be displaced. Hence, overall, gas filter pressing is not an effective way to facilitate melt loss and the formation of cumulates[52], although it could be an important means of redistributing fluid-mobile elements towards regions of ore deposition[85].

To summarize, cumulates are formed when melt and crystals are segregated from each other or when differentiation occurs through physical processes that act within the mush. Crystal–melt segregation results in igneous differentiation and spatial redistribution of incompatible or fluid-mobile elements. These changes can lead to the generation of eruptible melts and might result in ore mineralization.

Consequences of melt migration

The convective circulation of interstitial melts relative to their crystal framework has been relatively well researched, particularly for layered cumulates in dry basaltic mush systems. However, migration of melt through a mush framework does not need to be locally convective. Non-convective migration is thought to be a key driver of differentiation and crystal–melt segregation across chemically diverse mush systems[95,96]. In this section, we review the physical properties and chemical consequences of melt migration and explore feedbacks between melt migration and mush porosity.

Pervasive and channelized melt migration

The rate of porous melt migration (that is, movement of the interstitial liquid within the mush framework) depends on mush permeability, melt density and viscosity, and the pressure gradient driving the flow. The porosity, permeability and composition of crystal mushes are expected to vary on scales ranging from 10^{-3} m to 10^{3} m, owing to a combination of centimetre-scale modal layering and up to kilometre-scale primocryst phase layering found in many plutonic rocks[47,97,98]. Variations in texture and crystal packing characteristics (Box 1) can create melt fraction variations over the same range of length scales, leading to a spatially variable permeability. Additionally, the variation of melt fraction with temperature depends on the bulk composition, pressure and volatile (H_2O) contents[99] of the melt, which leads to further spatial variability in the rate of pervasive melt migration.

In addition to pervasive, grain-scale porous flow, many porous systems also display a second mode of porous flow through larger-scale, high-porosity features such as channels. Channelized flow is typical of industrial packed beds as well as natural systems such as the partially molten mantle where narrow channels and variable melt compositions can spontaneously develop[9,100]. Similar channel features also form in crystal mushes, for example, during melt–solid reactions[101–103], compositional convection[80] or fluid infiltration[90]. Additionally, channelization can develop dynamically during flow through porous mush, owing to reactive flow (that is, partial dissolution; Fig. 3a), which leads to reactive infiltration instabilities[100,104,105], or multiphase (immiscible) flow, which leads to viscous or capillary fingering[94,106]. Channelized features often occur on scales between the thin section and the outcrop scale, making it difficult to recognise the textural effects of channelized flow. It can therefore be challenging to understand the extent of channelization and to apply modelling approaches to interpret porous flow.

Buoyancy-driven pervasive melt migration might lead to instabilities in the form of melt-rich lenses[107,108], which can travel through the mush as porosity waves[49,95,107,109]. Such melt-rich lenses could be linked to rapid melt transport through, extraction from, or even creation of magma reservoirs[49,95,96,110]. Hence, slow (grain-scale) transport mechanisms could be physically linked to fast (channelized) transport mechanisms through porosity waves. Together these transport mechanisms could control melt distribution and extraction from mushes, providing a potential mechanism to understand magma formation timescales by drawing together chronological constraints and physics (see the section Crystal mush disaggregation and eruption).

The degree of textural equilibration between crystals and melt[67] is important for both pervasive and channelized porous melt migration because it affects the solid–melt dihedral angles and therefore controls the connectivity of the melt phase and the melt transfer rate.

The impact of deformation

In regions of active tectonism, shear deformation can substantially enhance melt flow and segregation[111]. Dilation of the pore spaces in the mush, which occurs when closely packed mush framework grains are forced apart to move past each other, is key to enhanced melt movement[55,111–113]. Dilation increases the volume of the pore spaces, locally reduces pressure in the interstitial melt and can suck in melt from

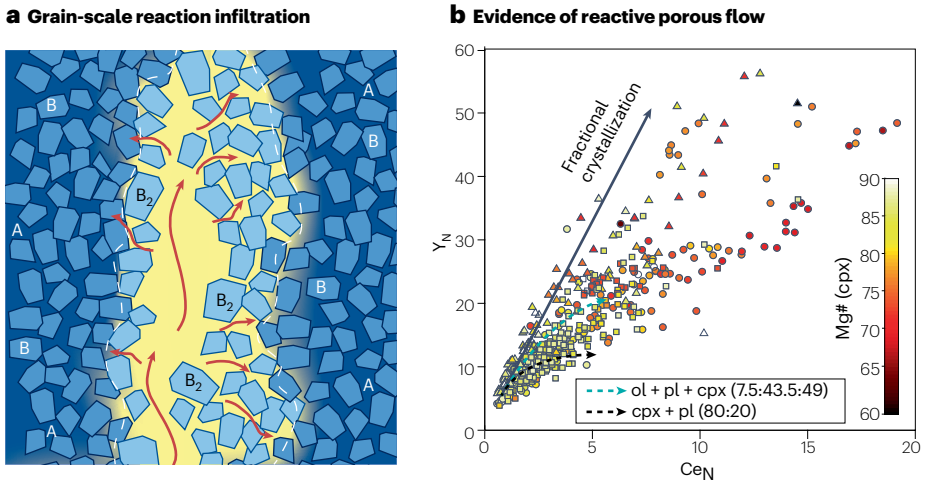

Fig. 3 | Reactive melt infiltration. a, A schematic illustration of grain-scale reaction infiltration of melt into a matrix of solid A + B (ref. 128). Melt (yellow) undersaturated in phase A (dark blue) infiltrates the mush (red arrows) and reacts with the solid matrix, causing dissolution of A and reprecipitation of new composition B_2, leading to channelization (outlined by the dashed white lines). **b**, Chondrite-normalized (N) compositions of Ce and Y in clinopyroxene (cpx) from global mid-ocean ridges (circles, East Pacific Rise; triangles, Mid-Atlantic Ridge; squares, South West Indian Ridge) are largely inconsistent with fractional crystallization (solid grey arrow) but can be reproduced through reactive melt flow (dotted blue arrow, with a solid modal assemblage of 7.5% olivine (ol) + 43.5% plagioclase (pl) + 49% cpx; dotted black arrow, with a solid modal assemblage of 80% cpx + 20% pl), based on refs. 101,102, updated using data from ref. 199. The colour bar shows the magnesium number (Mg# = Mg/(Mg + Fe)) for cpx. Reactive melt flow results in over-enrichment of trace elements relative to fractional crystallization and leads to recrystallization and chanelization. Part **b** adapted from ref. 101 under a Creative Commons licence CC BY 4.0.

surrounding areas[111,113,114]. Dilation during shear deformation causes melt to migrate away from grain boundaries normal to the maximum compressive stress, and into films or channels parallel to maximum compressive stress[55,113,115]. This migration is consistent with geodynamical and numerical modelling results, which show that tectonic extension favours vertical melt extraction[21,116]. Enhanced vertical melt extraction in extensional tectonic settings is consistent with the short timescales inferred petrologically for melt transfer in these settings[111,117–119]. Additionally, such migration could explain why magmas associated with upper-crustal compression have more differentiated chemistries than those associated with upper-crustal extension[119]. Thus, shear deformation can lead to local crystal–liquid segregation[113,120] and large-scale differentiation[9,39].

Reactive melt percolation

Much work has focused on the crystal–melt reactions that can accompany porous flow, because such reactions might have important implications for melt evolution[95,110,121,122]. These reactions can occur when a more evolved mush is replenished by more primitive melt[40,123,124] or during the migration of more evolved interstitial melt into a more primitive crystal mush[102,121].

If a replenishing melt is hotter than the mush or undersaturated in a phase present in the mush, it can trigger partial dissolution of the primocrysts, leading to increased mush porosity[110,125–127] (Fig. 3a). For example, partial dissolution can occur when pyroxene-saturated basaltic melts migrate through olivine-bearing mush[101,128], or when amphibole-saturated melts migrate through anhydrous assemblages[30,129]. Even if the migrating melt is saturated in the same phases present in the mush, the incoming melt is unlikely to be in chemical equilibrium with the framework crystals; for example, the melt might be saturated in olivine and plagioclase, but not be in equilibrium with the host magnesium/iron ratio and anorthite content. This disequilibrium triggers both diffusion-driven and dissolution–reprecipitation reactions. As a result, changes in modal abundance[101] and major, trace-element and isotopic composition are likely to occur between relict cores and new growth[102,124,127,129–132].

Reactive melt flow can be identified through its chemical effects on the mush. Fast-diffusing major elements in the percolating melt (such as iron and magnesium) can maintain equilibration with the crystal mush framework through diffusive exchange, whereas slower-diffusing elements cannot[101]. Furthermore, dissolution–reprecipitation reactions, which can occur in high-temperature experiments with run times as short as 6 h[133], might lead to an over-enrichment of incompatible trace elements in the melt relative to fractional crystallization trends[101,123] (Fig. 3b). These chemical signatures are common in plutonic systems, suggesting that reactive porous flow might contribute to melt evolution across various settings[30,102,121,123]. If the mush framework completely equilibrates with the melt for major elements, then this mush–melt equilibrium can be used for geobarometry to constrain the depths of mushy reservoirs[134].

Textural evidence for reactive flow typically includes the presence of relict cores and new rim compositions. However, these features can be difficult to distinguish from the products of some peritectic reactions[135,136]. For example, peritectic amphibole is formed during the differentiation of wet arc melts through reactions between clinopyroxene and olivine[102,135–137]. The rock record preserves textural and geochemical evidence of reactive melt percolation, from the micrometre scale in the Rum Layered Intrusion, Scotland[138] to at least the metre scale in the deep arc and oceanic crust[102,139]. To help identify and understand the impact of reactive flow, more work is needed to define the textural signatures that result when melt–mush reactions locally alter melt composition, porosity and permeability.

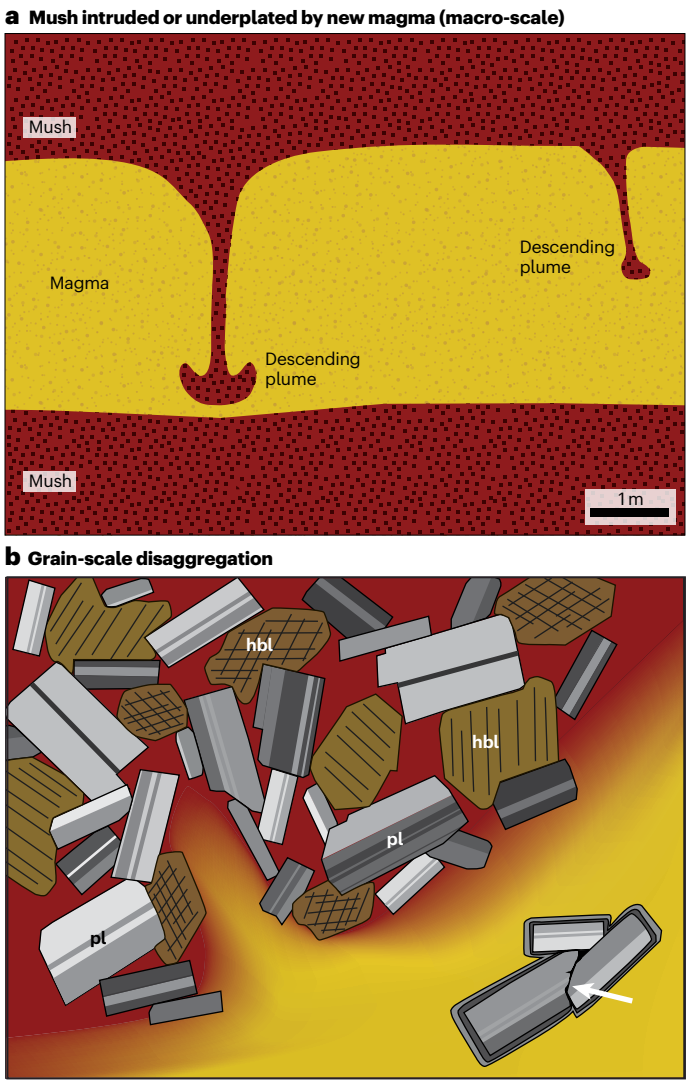

Fig. 4 | Mush disaggregation at different scales. a, Macro-scale Rayleigh–Taylor instabilities might cause plumes of crystal-rich material to descend from mush (red) intruded or underplated by new magma (yellow). The illustrative scale bar is approximately 1 m. **b**, Crystal-scale disaggregation of mush adjacent to melt-rich layer (yellow) results in the generation of antecrystic crystal cargo in the extracted magma. The glomerocryst represents a disaggregated fragment of the mush and shows evidence of dissolution at internal boundaries (arrow) and overgrowth rims that are common to all grains. Pre-eruptive processes can result in crystal mush disaggregation or destabilization. hbl, hornblende; pl, plagioclase.

Crystal–melt reactions during porous flow also affect the porosity of crystal mush, and thus have implications for melt transport, melt accumulation and mush stability. Thermodynamically constrained models for mafic systems show that recharge with primitive melt generally leads to net dissolution of mush phases and hence an increase in porosity[123,132]. For many scenarios of reactive flow of already-differentiated, interstitial melts in mafic crystal mush, thermodynamic modelling suggests that the ratio of assimilation to crystallisation is close to unity, indicating that porosity is maintained[132]. However, where plagioclase forms a large proportion of the reacted assemblage, porosity might decrease during the migration of evolved melts[132]. Reactive flow can alter mush porosity without requiring large increases in temperature[95,127], resulting in the formation of melt-rich lenses and potentially leading to mush destabilization and eruption. Overall, the evolution of the porosity and permeability of mush systems is governed by many complex physical and chemical factors; therefore, an integrated observational, experimental and modelling approach is required to fully understand it.

Crystal mush disaggregation and eruption

Volcanic eruptions occur when the internal pressure of the magma reservoir exceeds the external lithostatic pressure or the tensile strength of the host rock[140] and when the viscosity of the stored magma is low enough to allow flow, which is typically thought to be when the magma is melt dominated[14]. Evidence from geochronology and the mechanical understanding of mush behaviour suggests that crystal mushes primarily exist as a non-eruptible, rheologically locked crystal framework with interstitial melt[141–143]. This mush must be rejuvenated or reactivated to permit the eruption of crystal-rich mush or extraction of melt-rich magma from mush reservoirs. Therefore, in this section we discuss mechanisms of pre-eruptive mush rejuvenation and explore how these are expressed in erupted volcanic products.

Mush rejuvenation mechanisms

Mush rejuvenation could occur through mechanisms that are either internal or external to the reservoir[95,96]. In the case of rejuvenation by external recharge, a hot magma is intruded at the base of (or within) a mush and reactivates and weakens the crystal framework through partial melting[125,144,145]. This external rejuvenation is limited by the inefficiency of heat transfer[146,147] and is strongly dependent on the composition of the mush and magma; rejuvenation is favoured in wetter, rhyolitic mushes with hotter incoming magma[145]. Nonetheless, there are many examples across diverse tectonic settings in which mineral chemistry and thermometry indicate that heating has taken place shortly before eruption. In these cases, eruption is commonly inferred to have been caused (or immediately preceded) by replenishment of the reservoir by incoming magma, leading to extensive mush disaggregation[148–150]. Some mushes contain melt-rich layers from intrusion[126] or buoyancy-driven porous flow instabilities. In these cases, mush disaggregation could occur through Rayleigh–Taylor instabilities, which involve the descent of crystal-laden plumes into the melt-rich region[50,151] (Fig. 4a). Additionally, the percolation of exsolved hot volatiles through the crystal mush has been suggested to enhance heat transfer and buoyancy instabilities[90,146,152].

Mush rejuvenation through internal mechanisms occurs without any new magmatic input or external trigger. For example, enrichment of volatiles through fractionation could lead to nucleation of gas bubbles within the crystal framework[86]; alternatively a volatile-bearing mush with melt-rich layers might be intrinsically unstable[90,147,150,153]. The migration of melt-rich porosity wave instabilities through the mush could result in a locally increased melt fraction (that is, mush disaggregation) without requiring any external forcing[95,96]. In wet felsic systems, reactive melt flow might also increase the mush porosity enough to unlock the crystal mush and allow eruption[127,154]. Additionally, melt extraction through dyke generation is efficient in crystal-rich reservoirs[114]; therefore, mush derived crystal-poor magma can even form in systems in which the mush is not substantially disaggregated.

Any of these internally triggered events, which lead to destabilization or disaggregation of the crystal mush, could trigger eruptions in which the remnants of the parental mushes are entrained into the erupted magmas (Fig. 4b).

The crystal cargo

Mush reactivation leads to the incorporation of crystals that are potentially from different locations within a mushy reservoir, with different origins and histories, into erupted magma as crystal cargo[155]. Geochemical indicators of mush disaggregation cannot be identified from whole-rock compositions because the rocks represent a mixture of diverse crystal cargoes and melt(s). However, the diversity of materials found in erupted magmas provide petrological evidence for mushy subvolcanic storage systems. For example, plutonic and cumulate assemblages, brought to the surface as xenoliths and glomerocrysts or present in exposed crustal sections, show that crystal-rich mush zones are present within magmatic systems[26–29,156–159]. Additionally, disequilibrium mineral textures could indicate crystals that originated in a mush that underwent thermo-chemical rejuvenation and were then incorporated into an eruptible magma (Fig. 4b). These disequilibrium textures include sieve textured cores and strongly reversed zoning in crystal rims[24,31,35,160], as well as evidence for peritectic reactions or metastable phases[161,162]. These crystals are known as 'antecrysts' because they spent most of their history within the mush system but did not originate from the final erupted magma.

Elemental and isotopic variations within the crystal cargo also demonstrate the influx of new melt or the transfer of solids into new chemical environments during crystallization. Such open-system variations include reverse zoning and trace-element zoning that is inconsistent with major-element partitioning, and crystal-scale isotopic analyses that are not in isotopic equilibrium with the host melt. For example, observations of the Pb isotopic compositions of sanidine[163], in situ Sr isotopes in interstitial plagioclase[138], and Hf and O isotopic and trace elemental compositions of zircon[35,164] indicate crystal-scale isotopic disequilibrium between crystals and host melt, providing further evidence for open-system processes.

The crystal cargo can be used to calculate the timescales of storage, rejuvenation, or disruption of the mush and the release of free crystals into an eruptible magma (Fig. 4b). Radiometric ages of minerals are used to date crystallization times, and the typical pre-eruptive residence of crystals in volcanic rocks ranges from thousands of years (major primocrysts phases) to tens of thousands of years (zircon)[165]. In contrast, methods to quantify rejuvenation times include Ar/Ar dating of feldspar[166], computational modelling[145] and diffusion chronometry. Diffusion chronometry can be used to investigate various timescales: from years to hundreds of thousands of years using quartz[167–169] or plagioclase[170,171], hundreds to thousands of years using sanidine[169], years to thousands of years using clinopyroxene[172] or orthopyroxene[118,167], and minutes to months using Fe–Ti oxides[173]. However, the use of diffusion chronometry requires there to have been sufficient time between chemical perturbation and eruption for mineral rim growth to occur. Overall, evidence suggests that the timescales of rejuvenation can be rapid (days in many mafic systems or tens of years to thousands of years in more silicic systems).

The timescales deduced from diffusion chronometry commonly contradict the protracted timescales estimated for the establishment of the whole magmatic system[141–143]. This contrast between long storage timescales and short rejuvenation timescales has been attributed to the storage of magma as cold mush[141,142] with little interstitial melt, although combined zircon thermometry and geochronology work shows that some systems have larger melt fractions[174]. Alternatively, the application of diffusion chronometry relies on experimentally constrained diffusion coefficients; current lack of agreement between experimental studies means that diffusion timescales could reflect magma reservoir build up rather than eruption-related processes[168,171]. Otherwise, the apparent disparity in timescales might point towards an additional external mechanism for melt extraction, caused by features such as the regional stress field and/or pre-existing tectonic structures in active regions such as New Zealand[118,167,175] and the Southern Volcanic Zone of the Andes[119,176]. Improving quantitative constraints on temperature and timescales, for example, through modelling approaches, will help to understand the storage conditions of magmatic reservoirs within the crust throughout their lifetimes. Such developments could also provide an integrated perspective on all the steps involved in mush rejuvenation[145].

Crystal mush processes and crustal thermal maturity

Understanding the lifetimes of volcanic systems, patterns of intrusion and eruption, and the timescales and length scales of melt and crystal residence in the crust is essential to discern the future eruptive behaviour of volcanoes. Rejuvenation processes are crucial for allowing the mush system to evolve chemically. The prevalence and effectiveness of mush processes are affected by factors such as the thermal state of the crust, regional tectonic setting, and the mass and thermal balance of magma addition through intrusion into the crust. Additionally, mush processes can be limited by the textural character of the mush framework (Box 1) and the composition of the mush melt(s), which are linked to the crustal thermal state. In this section, we review how these factors affect mushes throughout the lifetime of a crustal volcanic system.

The thermal state of the crust

The thermal state of the crust is controlled by the balance of heat inputs and outputs. Heat inputs include the intrusion of mantle-derived melts, release of latent heat[123,127,177] and the redistribution of partial melt throughout the upper and lower crust[21,178]. Heat outputs include conductive cooling away from the magma, and hydrothermal circulation[177,179]. The thermal state of the crust therefore primarily depends on crustal thickness[180], mantle-derived melt fluxes, regional tectonics[21] and the distribution of radiogenic heat-producing species throughout the crust[181].

The thermal environment in the crust determines the cooling rate and crystal content of intrusions and governs the amount of time available for mush processes such as viscous compaction, melt extraction or porous melt migration. For example, ambient temperatures are higher in thick crust[96], leading to enhanced melt–solid differentiation[180]. Mafic to intermediate magmatism early in the lifetime of a volcanic system can thermally prime the crust, extending thermal equilibration times enough to allow the segregation of evolved melt, leading to the generation of silicic plutons[182]. The thermal environment also affects the amount of energy available for the assimilation of surrounding crust or remobilization of older, colder mushes. The thermal maturity of crust in volcanically active areas will change throughout the lifetime of the whole volcanic system[7,21,95,96,183] (Fig. 5). Therefore, the efficiency of mush processes is likely to vary over those lifetimes, depending on the thermal state of the crustal reservoir.

The thermal state also affects the textural maturity of the mush, which is likely to progress diffusively towards an increasingly

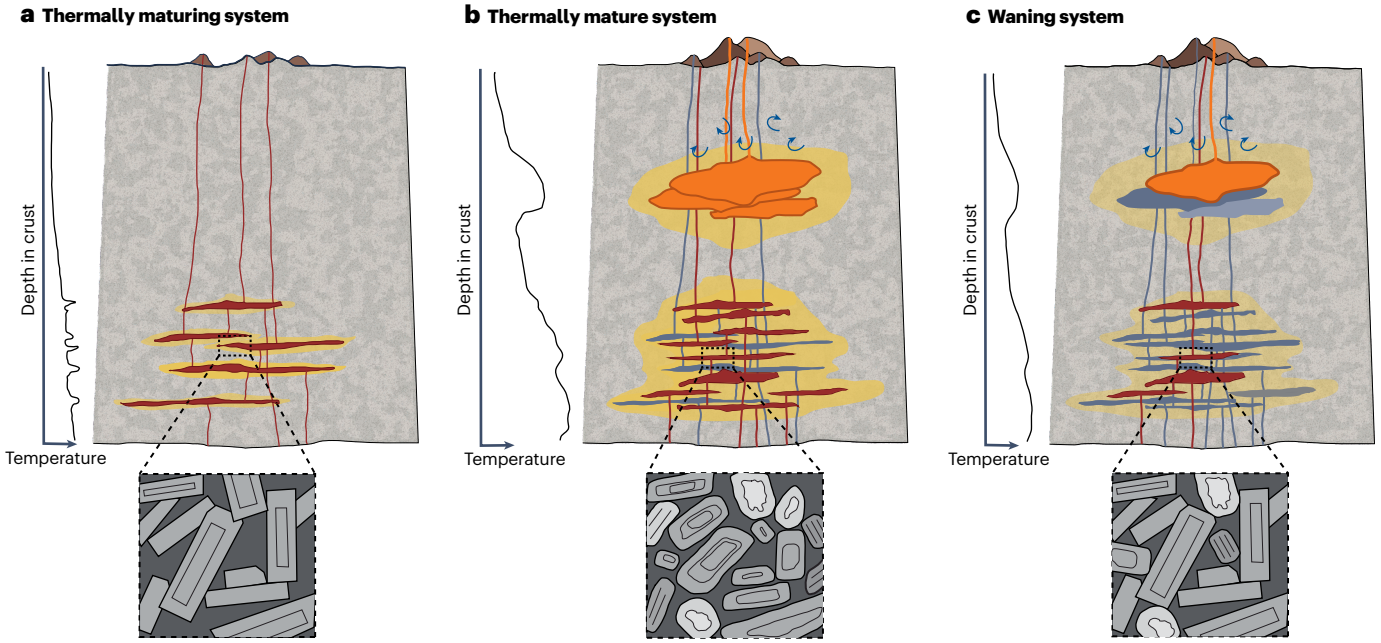

Fig. 5 | Conceptual life cycle of a crustal magmatic system. a, The key features, schematic temperature profile through the centre of the panel (left axis) and possible textural features of a developing mush (inset) for a thermally maturing system. The vertical lines represent dykes. The horizontal bodies (dark red) are sills. **b**, As in **a**, but for a thermally mature system in which evolved magma (orange) is emplaced at mid- to upper-crustal levels. Thick margins denote colder boundaries. The curving blue arrows indicate hydrothermal circulation. Older, inactive intrusive bodies are shown in blue-grey. **c**, As in **b**, but for a waning system. The overall crustal temperature increases and becomes less localized as systems become thermally mature, leading to widespread mush and extensive partial melting and crustal assimilation (yellow regions) in thermally mature systems. Crystal textures might be unequilibrated in maturing systems, becoming more equilibrated and more equant following repeated intrusion, resorption, rejuvenation and recrystallization during thermal maturation, resulting in a complex crystal cargo. Individual intrusions cool quickly in immature systems but can be maintained for longer periods as the system matures. The waning system reverts to more localized heat distribution and lower overall ambient temperatures, but retains some of the complex crystal cargo and high assimilation rates.

connected melt phase[29] (Box 1). Long-lived (mature) mush systems (from 0.1 to 10 Myr (refs. 142,143,184)) are expected to tend towards more mature crystal textures and melt geometries (lower dihedral angles[67]). These long-lived systems experience repeated episodes of heating, resorption and recrystallization[7,90,142,143], causing the shapes of crystals in mushes to evolve towards more equant character, closer to equilibrium (Wulff) crystal shapes[13].

Thermally immature systems. In thermally immature (maturing) systems (Fig. 5a), each intrusion cools quickly[7,95,96]. In such systems, individual intrusion events generate packets of crystal mush that are short lived. These events produce only limited amounts of extracted evolved melt[110] and cause limited local melting and assimilation of the crust[95,183]. The short-lived mush, less-equilibrated textures and low overall ambient temperatures of thermally immature crust lead to limited opportunity for viscous compaction, mechanical rearrangement or porous melt migration in the early stages of a volcanic system (the 'incubation stage'[95]). Immature or young systems are unlikely to sustain large upper-crustal magma chambers[21,178].

Thermally mature systems. The crust can reach thermal maturity within approximately 1 Myr (refs. 95,110,116,185) for geologically reasonable melt fluxes (Fig. 5b). Thermally mature systems have high ambient temperature and high melt flux, enabling them to maintain magmatic systems above the solidus for extended periods of times, perhaps exceeding 10^5 yr (refs. 179,186,187). Texturally mature mush (Box 1) has smoothly curving grain boundaries and continuous grain boundary melt films. These features facilitate effective porous melt migration even at low melt fractions[68,188] and lead to mass transfer, melt differentiation and reactive flow[95,127,173]. Evidence for these processes has been identified in the geological record in deep-seated crustal systems[101,102,123]. Thermal maturation increases the extent of crustal assimilation, as indicated by diverse modelling approaches[95,110,116] and through isotopic analysis combined with geochronology of mid-upper-crustal plutons[189,190].

Many middle to upper-crustal reservoirs receive magmatic inputs directly from lower crustal mushes[178,191,192] (Fig. 5b), and themselves represent long-lived silicic mush systems (for example, the Altiplano Puna Magma Body[3]). Some upper-crustal reservoirs beneath composite volcanoes generate evolved products directly from primitive melt through a long-lived crystal mush[191,193].

Thermally waning systems. The waning stages of magmatic systems (Fig. 5c) are under-represented in the literature. Existing research suggests that these systems experience an overall decrease in heat input, mass eruption rates and magmatic temperatures[184,189,193], and might be associated with a return to increasingly mafic volcanism[110,189,194]. Waning systems might also exhibit more assimilation of lower crustal

cumulates and residual mushes compared with recharge[195,196]. The temporal progression of magmatic systems is challenging to investigate because in plutonic rocks, preserved magmatic structures might be dominated by the most voluminous or later stages of magmatism; the magmatic record of melt chemistry might also be progressively overprinted and masked by later activity[183].

The regional tectonic environment

Coupled with the thermal structure of the crust, regional tectonics has an important role in controlling crystal mush development. For example, extensional tectonics imparts a shear stress on the crust, which is thought to drive rapid vertical melt extraction[111,113,117–119]. Extension also perturbs the geotherm, increasing the extent of melting and allowing the advection of magma into the upper crust[21]. Conversely, compressional tectonics inhibit the ascent of buoyant magma through dyking and therefore enhance magma intrusion[197].

The properties of melts produced vary between cool and wet (arc) settings compared with hot and dry (extensional or hot spot) settings. For example, the relationship between temperature and crystallinity varies with the melt composition and water content, and determines how long residual melt can persist in the system[21] (Fig. 6). A dry tholeiitic melt could crystallize fully over a temperature interval of <150 °C, whereas a wet andesitic melt could still contain melt after 450 °C of cooling (Fig. 6). Therefore, crystal mush in deep arc crust might persist longer than crystal mush in a shallow oceanic crust, allowing more crystal–melt segregation, viscous compaction and assimilation of older mush material. Additionally, water-rich melt has a lower viscosity than dry melt and is therefore more easily segregated at a given mush crystal fraction and more likely to form isolated melt-rich lenses[198]. The importance of water content extends to upper-crustal mushes: the ratio of exsolved volatile content to crystal content impacts whether volatiles are transported through stable intercrystalline pathways or retained as a dispersed phase. These transport properties affect the efficiency of outgassing and the buoyancy of the bulk mush[90], and might modulate the explosivity of resulting volcanic activity.

Summary and future perspectives

Crystal mushes are a ubiquitous feature of all crystallizing magma bodies. The physical properties of crystal mushes are defined by their grain-scale structure and are expected to vary spatially. Mush behaviour is highly complex and involves nonlinear feedbacks: mushes are characterized by the flow of heat, momentum and chemical species on various spatial and temporal scales. Melt migrates within crystal mushes through pervasive and channelized flow, leading to reactions with the crystalline framework and dynamic instabilities. Disaggregation of mushes through pre-eruptive processes generates a crystal cargo found in volcanic rocks. Understanding the properties and behaviour of crystal mushes is an important focus for research into volcanic and magmatic systems.

The permeability and rheology of a crystal mush depend on its pore-scale to metre-scale characteristics, including the degree of textural equilibration between crystals and melt. Characterization of the rheology of mushes with realistic grain shapes and size dispersions is needed to understand the timescales and length scales of melt extraction and infiltration processes. However, existing theoretical and experimental work has typically focused on simple, monodispersed grain shapes, maximally dense grain packings and frictionless systems. Techniques such as X-ray tomography, numerical modelling and two-dimensional trace elemental geochemical mapping can directly characterize how porosity and permeability evolve as natural mushes crystallize, although discriminating between phases remains challenging. Thus, efforts to improve the empirical, theoretical and experimental characterization of natural crystal packings are needed to robustly link field observations and textural evidence with physics and chemical reactivity. Fields such as engineering and metallurgy involve aligned processes in crystallizing alloys, such as slurry flow and hot tearing. Engaging with researchers in these fields to apply understanding of these processes to natural silicate mushes could also help to improve understanding of crystal mush behaviour.

Mush compaction is highly relevant to the rates of cumulate formation, mush evolution and the extraction of melt to form upper-crustal magmatic systems; however, it remains poorly understood. A wide-ranging investigation of varied natural plutonic settings is needed to improve understanding of mush compaction. The onset, spatial extent and orientation of compaction are likely to depend on the size, shape and orientation of the crystals in the mush, and the temperature and longevity of each system. A key goal is therefore to link chemistry and deformation on length scales ranging from grain-scale to intrusion-scale with the three-dimensional orientation of crystal zoning textures or crystal defects as defined by techniques such as electron backscatter diffraction. The relative importance and timescales of

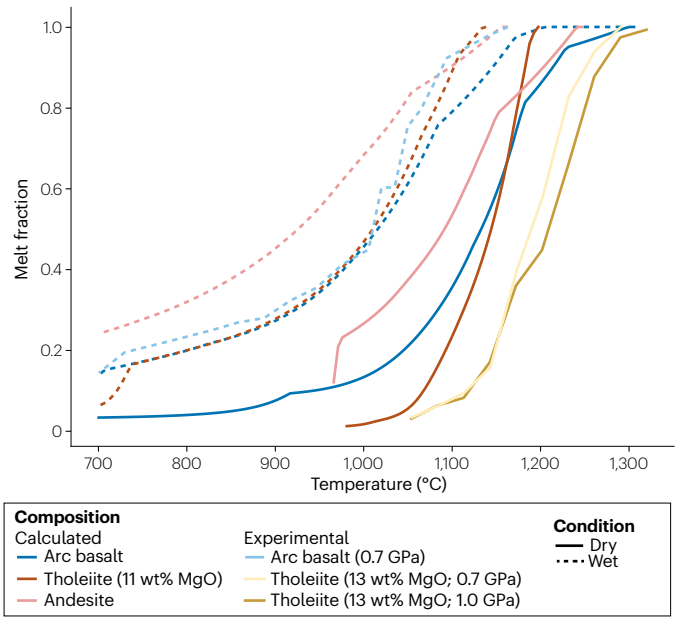

Fig. 6 | The relationship between temperature and melt fraction. The dependence of melt fraction on temperature calculated for wet melts (dashed lines, containing 2 wt% H_2O at the liquidus temperature) and dry melts (solid lines) using the thermodynamic Gibbs free energy minimization package MAGEMin[200] with the Thermocalc igneous thermodynamic database[201]. Fractional crystallization is simulated under quartz–fayalite–magnetite equilibrium oxygen fugacity conditions at a pressure of 0.5 GPa, using 5 °C temperature increments and taking the residue as the new bulk composition for the next step. The andesite, tholeiite and arc basalt starting compositions are from ref. 202, ref. 203 and ref. 204, respectively. Experimental constraints for tholeiite (dry at 0.7 GPa (ref. 205) and dry at 1.0 GPa (ref. 206)) and arc basalt (wet at 0.7 GPa (ref. 207)) are shown for comparison. Wet mushes retain melt over much longer temperature intervals than dry mushes.

Glossary

Adcumulate rocks
rocks dominated by unzoned, interstitial overgrowths of the primocryst phases with minimal amounts of trapped pore material.

Assimilation
the incorporation of surrounding crust into magma.

Compaction length scale
the characteristic distance over which the compaction rate decreases by a factor e.

Diffusion chronometry
the process of extracting time information about magmatic processes from diffusive changes in chemical gradients.

Force chain
a network of linked particles that carry more than the average load in a mush.

Glomerocryst
a texturally distinct polycrystalline aggregate of macroscopic crystals within a volcanic rock.

Igneous differentiation
any process by which magmas can change their bulk composition.

Loosely packed mush
a loose aggregate of solid particles that can be densified if the particles are rearranged.

Maximum packing
a dense packing of particles that cannot be densified without deformation of the particles.

Percolation threshold
the porosity limit above which percolative flow can no longer occur through a porous medium.

Primocryst
a crystal formed in the early stages of fractionation that makes up part of the crystal mush framework.

Rayleigh number
a dimensionless number that describes the ratio between thermal buoyancy and diffusion, and thus the likelihood of convection.

Rejuvenation
the mobilization of mushy material through the addition of heat or changes in porosity.

Rheology
the study of material deformation and flow.

compaction, mechanical consolidation and melt extraction could be investigated by combining these petrographic and textural constraints with isotopic dating and numerical modelling.

Numerical modelling and rheology work emphasize the importance of larger-scale melt migration features such as porosity waves and channelization. However, these features are difficult to capture through petrological analysis and it is unclear whether they are geophysically detectable. Understanding of reactive melt migration is in its infancy, and many open questions remain. One important question is whether reactive flow is a fundamental feature of melt transport and accumulation, or if it predominantly occurs in mush reservoirs as porosity is decreasing and the system is freezing. Additionally, the mechanisms, timescales and chemical effects of reactive flow need to be better constrained to understand the compositional evolution of melts. Making progress on these issues demands an integrated experimental and theoretical (modelling) framework for reactive flow that can be benchmarked against natural observations. Developing such a framework will require advances in numerical methods for coupling reactions and transport, and in thermodynamic frameworks that can capture the full phase equilibria of natural systems.

Crystal mushes span various length scales. Therefore, reservoir-scale models should be complemented by grain-scale to meso-scale modelling to capture the full range of complexity in the governing processes. This development will require numerical schemes that can link the macro- and microphysics of granular material, as well as diffusive relaxation of elements or isotopes. The outputs from such models should be integrated with field-based observations and petrology. Experiments can provide important inputs to models by constraining mechanisms and rates of crystal–melt reactions, but multicomponent thermodynamic frameworks will be needed to ensure that the models and in situ geochemistry match. Additionally, case studies of plutonic and volcanic systems, combining spatially constrained elemental and isotopic data, can help reconstruct the evolution of porosity and permeability as a function of composition and temperature, and constrain the length scale and time scale of porous flow.

Pre-eruptive volcanic processes are sampled through disaggregation of crystal mush into crystal cargo in ascending magmas, but these mechanisms are poorly understood. There is a need to explore further the mechanisms of pre-eruptive mush disaggregation, which could include a combination of larger-scale fluid dynamical instabilities, local grain-scale remelting, or melt reaction and infiltration. Scaled analogue experiments and numerical models would help to constrain the dynamics of these processes, permitting interpretation of the timescales of mush storage, rejuvenation and disruption, as defined through diffusion chronometry in the crystal cargo.

Volcanic systems involve multiple interacting timescales reflecting competing processes across different spatial scales. Crystal mush processes can be sampled at length scales ranging from tens of kilometres (through geophysical observations, continuum scale numerical modelling, geological mapping and bulk rock geochemistry) to micrometres (using crystal-scale textures, geochemistry and pore-scale numerical modelling). However, the different length scale of focus for each mode of investigation makes it difficult to integrate information across different techniques. There is a need to integrate data obtained from petrology, geochemistry and advanced geophysical techniques (such as full waveform seismic inversion) with numerical modelling and understanding of the dynamics of multiphase granular materials. Combining this information with detailed field and geochronology work would improve understanding of the importance of mush processes across long timescales throughout the life cycle of whole magmatic systems.

Published online: 3 June 2025

References

1. Marsh, B. D. Solidification fronts and magmatic evolution. *Mineral. Mag.* **60**, 5–40 (1996).
2. Magee, C. et al. Magma plumbing systems: a geophysical perspective. *J. Petrol.* **59**, 1217–1251 (2018).
3. Ward, K. M., Zandt, G., Beck, S. L., Christensen, D. H. & McFarlin, H. Seismic imaging of the magmatic underpinnings beneath the Altiplano-Puna volcanic complex from the joint inversion of surface wave dispersion and receiver functions. *Earth Planet. Sci. Lett.* **404**, 43–53 (2014).
4. Paulatto, M. et al. Advances in seismic imaging of magma and crystal mush. *Front. Earth Sci.* https://doi.org/10.3389/feart.2022.970131 (2022).
5. Cashman, K. V., Sparks, R. S. J. & Blundy, J. D. Vertically extensive and unstable magmatic systems: a unified view of igneous processes. *Science* **355**, eaag3055 (2017).
6. Bachmann, O. & Bergantz, G. W. On the origin of crystal-poor rhyolites: extracted from batholithic crystal mushes. *J. Petrol.* **45**, 1565–1582 (2004).
7. Annen, C., Blundy, J. & Sparks, R. The genesis of intermediate and silicic magmas in deep crustal hot zones. *J. Petrol.* **47**, 505–539 (2006).
8. Sparks, R. et al. Formation and dynamics of magma reservoirs. *Philos. Trans. R. Soc. A* **377**, 20180019 (2019).
9. Weinberg, R. F., Vernon, R. H. & Schmeling, H. Processes in mushes and their role in the differentiation of granitic rocks. *Earth Sci. Rev.* **220**, 103665 (2021).

10. Mueller, S., Llewellin, E. & Mader, H. The rheology of suspensions of solid particles. *Proc. R. Soc. A* **466**, 1201–1228 (2010).
11. Vigneresse, J. L., Barbey, P. & Cuney, M. Rheological transitions during partial melting and crystallization with application to felsic magma segregation and transfer. *J. Petrol.* **37**, 1579–1600 (1996).
12. Bohrson, W. A. et al. Thermodynamic model for energy-constrained open-system evolution of crustal magma bodies undergoing simultaneous recharge, assimilation and crystallization: the magma chamber simulator. *J. Petrol.* **55**, 1685–1717 (2014).
13. Mangler, M. F. et al. Crystal resorption as a driver for mush maturation: an experimental Investigation. *J. Petrol.* **65**, egae088 (2024).
14. Marsh, B. D. On the crystallinity, probability of occurrence, and rheology of lava and magma. *Contrib. Mineral. Petrol.* **78**, 85–98 (1981).
15. Eichelberger, J. Distribution and transport of thermal energy within magma–hydrothermal systems. *Geosciences* **10**, 212 (2020).
16. O'Driscoll, B., Emeleus, C. H., Donaldson, C. H. & Daly, J. S. Cr-spinel seam petrogenesis in the Rum Layered Suite, NW Scotland: cumulate assimilation and in situ crystallization in a deforming crystal mush. *J. Petrol.* **51**, 1171–1201 (2010).
17. Larsen, L. M. & Sørensen, H. The Ilímaussaq intrusion — progressive crystallization and formation of layering in an agpaitic magma. *Geol. Soc. Spec. Publ.* **30**, 473–488 (1987).
18. Nielsen, T. F. et al. The Skaergaard PGE and gold deposit: the result of in situ fractionation, sulphide saturation, and magma chamber-scale precious metal redistribution by immiscible Fe-rich melt. *J. Petrol.* **56**, 1643–1676 (2015).
19. Buret, Y. et al. From a long-lived upper-crustal magma chamber to rapid porphyry copper emplacement: reading the geochemistry of zircon crystals at Bajo de la Alumbrera (NW Argentina). *Earth Planet. Sci. Lett.* **450**, 120–131 (2016).
20. Iyer, H. M. Geophysical evidence for the locations, shapes and sizes, and internal structures of magma chambers beneath regions of Quaternary volcanism. *Phil. Trans. R. Soc. A* **310**, 473–510 (1984).
21. Karakas, O. & Dufek, J. Melt evolution and residence in extending crust: thermal modeling of the crust and crustal magmas. *Earth Planet. Sci. Lett.* **425**, 131–144 (2015).
22. Mullet, B. & Segall, P. The surface deformation signature of a transcrustal, crystal mush-dominant magma system. *JGR Solid Earth* **127**, e2022JB024178 (2022).
23. Arculus, R. J. & Wills, K. J. A. The petrology of plutonic blocks and inclusions from the Lesser Antilles Island arc. *J. Petrol.* **21**, 743–799 (1980).
24. Bennett, E. N., Lissenberg, C. J. & Cashman, K. V. The significance of plagioclase textures in mid-ocean ridge basalt (Gakkel Ridge, Arctic Ocean). *Contrib. Mineral. Petrol.* **174**, 1–22 (2019).
25. Tait, S. R., Wörner, G., Van Den Bogaard, P. & Schmincke, H.-U. Cumulate nodules as evidence for convective fractionation in a phonolite magma chamber. *J. Volcanol. Geotherm. Res.* **37**, 21–37 (1989).
26. Holness, M. B. et al. Textures in partially solidified crystalline nodules: a window into the pore structure of slowly cooled mafic intrusions. *J. Petrol.* **48**, 1243–1264 (2007).
27. Horn, E. L., Taylor, R. N., Gernon, T. M., Stock, M. J. & Farley, E. R. Composition and petrology of a mush-bearing magma reservoir beneath Tenerife. *J. Petrol.* **63**, egac095 (2022).
28. Kiddle, E. et al. Crustal structure beneath Montserrat, Lesser Antilles, constrained by xenoliths, seismic velocity structure and petrology. *Geophys. Res. Lett.* **37**, L00E11 (2010).
29. Holness, M. B., Stock, M. J. & Geist, D. Magma chambers versus mush zones: constraining the architecture of sub-volcanic plumbing systems from microstructural analysis of crystalline enclaves. *Philos. Trans. R. Soc. A* **377**, 20180006 (2019).
30. Cooper, G. F., Davidson, J. P. & Blundy, J. D. Plutonic xenoliths from Martinique, Lesser Antilles: evidence for open system processes and reactive melt flow in island arc crust. *Contrib. Mineral. Petrol.* **171**, 87 (2016).
31. Neave, D. A., Buisman, I. & Maclennan, J. Continuous mush disaggregation during the long-lasting Laki fissure eruption, Iceland. *Am. Min.* **102**, 2007–2021 (2017).
32. Holness, M. B., Humphreys, M. C., Sides, R., Helz, R. T. & Tegner, C. Toward an understanding of disequilibrium dihedral angles in mafic rocks. *J. Geophys. Res. Solid Earth* **117**, B06207 (2012).
33. Helz, R. T. Crystallization history of Kilauea Iki lava lake as seen in drill core recovered in 1967–1979. *Bull. Volcanol.* **43**, 675–701 (1980).
34. Lesher, C. E. & Walker, D. Cumulate maturation and melt migration in a temperature gradient. *J. Geophys. Res.* **93**, 10295–10311 (1988).
35. Wallrich, B. et al. Volcano–pluton connection: perspectives on material and process linkages, searchlight pluton and Highland Range volcanic sequence, Nevada, USA. *Earth Sci. Rev.* **238**, 104361 (2023).
36. Holness, M. B. et al. Crystal mush growth and collapse on a steep wall: the marginal border series of the Skaergaard Intrusion, East Greenland. *J. Petrol.* **63**, egab100 (2022).
37. Alasino, P. H., Ardill, K. E. & Paterson, S. R. Magmatic faults: challenges, progress, and possibilities. *Earth Sci. Rev.* **260**, 104992 (2025).
38. Vernon, R. & Collins, W. Structural criteria for identifying granitic cumulates. *J. Geol.* **119**, 127–142 (2011).
39. Garibaldi, N., Tikoff, B., Schaen, A. J. & Singer, B. S. Interpreting granitic fabrics in terms of rhyolitic melt segregation, accumulation, and escape via tectonic filter pressing in the Huemul Pluton, Chile. *J. Geophys. Res. Solid Earth* **123**, 8548–8567 (2018).
40. Bédard, J. H. Cumulate recycling and crustal evolution in the Bay of Islands ophiolite. *J. Geol.* **99**, 225–249 (1991).
41. Kerr, R. C. & Lister, J. R. The effects of shape on crystal settling and on the rheology of magmas. *J. Geol.* **99**, 457–467 (1991).
42. Druitt, T. Settling behaviour of concentrated dispersions and some volcanological applications. *J. Volcanol. Geotherm. Res.* **65**, 27–39 (1995).
43. Schwindinger, K. R. Particle dynamics and aggregation of crystals in a magma chamber with application to Kilauea Iki olivines. *J. Volcanol. Geotherm. Res.* **88**, 209–238 (1999).
44. Suckale, J., Sethian, J. A., Yu, J. & Elkins-Tanton, L. T. Crystals stirred up: 1. Direct numerical simulations of crystal settling in nondilute magmatic suspensions. *J. Geophys. Res.* **117**, E08004 (2012).
45. Bons, P. D. et al. Layered intrusions and traffic jams. *Geology* **43**, 71–74 (2015).
46. Manoochehri, S. & Schmidt, M. W. Settling and compaction of chromite cumulates employing a centrifuging piston cylinder and application to layered mafic intrusions. *Contrib. Mineral. Petrol.* **168**, 1–20 (2014).
47. Namur, O. et al. in *Layered Intrusions* (eds Charlier, B. et al.) 75–152 (Springer, 2015).
48. Snabre, P., Pouligny, B., Metayer, C. & Nadal, F. Size segregation and particle velocity fluctuations in settling concentrated suspensions. *Rheol. Acta* **48**, 855–870 (2009).
49. Wong, Y.-Q. & Keller, T. A unified numerical model for two-phase porous, mush and suspension flow dynamics in magmatic systems. *Geophys. J. Int.* **233**, 769–795 (2023).
50. Michioka, H. & Sumita, I. Rayleigh–Taylor instability of a particle packed viscous fluid: implications for a solidifying magma. *Geophys. Res. Lett.* **32**, L03309 (2005).
51. Holness, M. B. Melt segregation from silicic crystal mushes: a critical appraisal of possible mechanisms and their microstructural record. *Contrib. Mineral. Petrol.* **173**, 48 (2018).
52. Bachmann, O. & Huber, C. The inner workings of crustal distillation columns; the physical mechanisms and rates controlling phase separation in silicic magma reservoirs. *J. Petrol.* **60**, 3–18 (2019).
53. Florez, D. et al. Repacking in compacting mushes at intermediate melt fractions: constraints from numerical modeling and phase separation experiments on granular media. *JGR Solid Earth* **129**, e2024JB029077 (2024).
54. Couturier, É., Boyer, F., Pouliquen, O. & Guazzelli, É. Suspensions in a tilted trough: second normal stress difference. *J. Fluid Mech.* **686**, 26–39 (2011).
55. Bergantz, G. W., Schleicher, J. M. & Burgisser, A. On the kinematics and dynamics of crystal-rich systems. *J. Geophys. Res. Solid Earth* **122**, 6131–6159 (2017).
56. Hoyos, S., Florez, D., Pec, M. & Huber, C. Crystal shape control on the repacking and jamming of crystal-rich mushes. *Geophys. Res. Lett.* **49**, e2022GL100040 (2022).
57. Renner, J., Viskupic, K., Hirth, G. & Evans, B. Melt extraction from partially molten peridotites. *Geochem. Geophys. Geosyst.* https://doi.org/10.1029/2002GC000369 (2003).
58. Hartung, E. et al. Evidence for residual melt extraction in the takidani pluton, central Japan. *J. Petrol.* **58**, 763–788 (2017).
59. Cuetos, A., Dennison, M., Masters, A. & Patti, A. Phase behaviour of hard board-like particles. *Soft Matter* **13**, 4720–4732 (2017).
60. Meurer, W. & Boudreau, A. Compaction of igneous cumulates part I: geochemical consequences for cumulates and liquid fractionation trends. *J. Geol.* **106**, 281–292 (1998).
61. Meurer, W. & Boudreau, A. Compaction of igneous cumulates part II: compaction and the development of igneous foliations. *J. Geol.* **106**, 293–304 (1998).
62. Cooper, R. & Kohlstedt, D. Solution-precipitation enhanced diffusional creep of partially molten olivine-basalt aggregates during hot-pressing. *Tectonophysics* **107**, 207–233 (1984).
63. Tharp, T. M., Loucks, R. R. & Sack, R. O. Modeling compaction of olivine cumulates in the Muskox intrusion. *Am. J. Sci.* **298**, 758–790 (1998).
64. Ribe, N. M. Theory of melt segregation — a review. *J. Volcanol. Geotherm. Res.* **33**, 241–253 (1987).
65. McKenzie, D. The generation and compaction of partially molten rock. *J. Petrol.* **25**, 713–765 (1984).
66. McKenzie, D. Compaction and crystallization in magma chambers: towards a model of the skaergaard intrusion. *J. Petrol.* **52**, 905–930 (2011).
67. Holness, M. B., Cheadle, M. J. & McKenzie, D. On the use of changes in dihedral angle to decode late-stage textural evolution in cumulates. *J. Petrol.* **46**, 1565–1583 (2005).
68. Cheadle, M., Elliott, M. & McKenzie, D. Percolation threshold and permeability of crystallizing igneous rocks: the importance of textural equilibrium. *Geology* **32**, 757–760 (2004).
69. Keller, T. & Suckale, J. A continuum model of multi-phase reactive transport in igneous systems. *Geophys. J. Int.* **219**, 185–222 (2019).
70. Lee, C.-T. A. & Morton, D. M. High silica granites: terminal porosity and crystal settling in shallow magma chambers. *Earth Planet. Sci. Lett.* **409**, 23–31 (2015).
71. Holness, M. B., Vukmanovic, Z. & Mariani, E. Assessing the role of compaction in the formation of adcumulates: a microstructural perspective. *J. Petrol.* **58**, 643–673 (2017).
72. Boudreau, A. E. & McBirney, A. R. The Skaergaard layered series. Part III. Non-dynamic layering. *J. Petrol.* **38**, 1003–1020 (1997).
73. Bertolett, E., Prior, D., Gravley, D., Hampton, S. & Kennedy, B. Compacted cumulates revealed by electron backscatter diffraction analysis of plutonic lithics. *Geology* **47**, 445–448 (2019).
74. Namur, O. & Charlier, B. Efficiency of compaction and compositional convection during mafic crystal mush solidification: the Sept Iles layered intrusion, Canada. *Contrib. Mineral. Petrol.* **163**, 1049–1068 (2012).
75. Lissenberg, C. J., MacLeod, C. J. & Bennett, E. N. Consequences of a crystal mush-dominated magma plumbing system: a mid-ocean ridge perspective. *Philos. Trans. R. Soc. A* **377**, 20180014 (2019).

76. Yao, Z., Qin, K. & Xue, S. Kinetic processes for plastic deformation of olivine in the Poyi ultramafic intrusion, NW China: insights from the textural analysis of a ~1700 m fully cored succession. *Lithos* **284**, 462–476 (2017).
77. Ferrando, C. et al. Role of compaction in melt extraction and accumulation at a slow spreading center: microstructures of olivine gabbros from the Atlantis Bank (IODP Hole U1473A, SWIR). *Tectonophysics* **815**, 229001 (2021).
78. Vukmanovic, Z., Holness, M. B., Stock, M. J. & Roberts, R. J. The creation and evolution of crystal mush in the upper zone of the Rustenburg Layered Suite, Bushveld Complex, South Africa. *J. Petrol.* **60**, 1523–1542 (2019).
79. Tait, S. R., Huppert, H. E. & Sparks, R. S. J. The role of compositional convection in the formation of adcumulate rocks. *Lithos* **17**, 139–146 (1984).
80. Tait, S. & Jaupart, C. Compositional convection in a reactive crystalline mush and melt differentiation. *J. Geophys. Res.* **97**, 6735–6756 (1992).
81. Kerr, R. C. & Tait, S. R. Crystallization and compositional convection in a porous medium with application to layered igneous intrusions. *J. Geophys. Res.* **91**, 3591–3608 (1986).
82. Petford, N. in *Flow and Creep in the Solar System: Observations, Modeling and Theory* (eds Stone, D. B. & Runcorn, S. K.) 261–286 (Springer, 1993).
83. Wager, L. R., Brown, G. M. & Wadsworth, W. J. Types of igneous cumulates. *J. Petrol.* **1**, 73–85 (1960).
84. Sparks, R. S. J., Huppert, H. E., Kerr, R., McKenzie, D. & Tait, S. R. Postcumulus processes in layered intrusions. *Geol. Mag.* **122**, 555–568 (1985).
85. Vigneresse, J.-L., Truche, L. & Richard, A. How do metals escape from magmas to form porphyry-type ore deposits? *Ore Geol. Rev.* **105**, 310–336 (2019).
86. Humphreys, M. C. et al. Rapid pre-eruptive mush reorganisation and atmospheric volatile emissions from the 12.9 ka Laacher See eruption, determined using apatite. *Earth Planet. Sci. Lett.* **576**, 117198 (2021).
87. Pistone, M. et al. Gas-driven filter pressing in magmas: insights into in-situ melt segregation from crystal mushes. *Geology* **43**, 699–702 (2015).
88. Boudreau, A. Bubble migration in a compacting crystal-liquid mush. *Contrib. Mineral. Petrol.* **171**, 1–17 (2016).
89. Sisson, T. W. & Bacon, C. R. Gas-driven filter pressing in magmas. *Geology* **27**, 613–616 (1999).
90. Parmigiani, A., Huber, C. & Bachmann, O. Mush microphysics and the reactivation of crystal-rich magma reservoirs. *J. Geophys. Res. Solid Earth* **119**, 6308–6322 (2014).
91. Degruyter, W., Parmigiani, A., Huber, C. & Bachmann, O. How do volatiles escape their shallow magmatic hearth? *Philos. Trans. R. Soc. A* **377**, 20180017 (2019).
92. Belien, I. B., Cashman, K. V. & Rempel, A. W. Gas accumulation in particle-rich suspensions and implications for bubble populations in crystal-rich magma. *Earth Planet. Sci. Lett.* **297**, 133–140 (2010).
93. Huber, C. & Parmigiani, A. A physical model for three-phase compaction in silicic magma reservoirs. *J. Geophys. Res. Solid Earth* **123**, 2685–2705 (2018).
94. Lenormand, R., Touboul, E. & Zarcone, C. Numerical models and experiments on immiscible displacements in porous media. *J. Fluid Mech.* **189**, 165–187 (1988).
95. Jackson, M., Blundy, J. & Sparks, R. Chemical differentiation, cold storage and remobilization of magma in the Earth's crust. *Nature* **564**, 405–409 (2018).
96. Solano, J. M. S., Jackson, M. D., Sparks, R. S. J., Blundy, J. D. & Annen, C. Melt segregation in deep crustal hot zones: a mechanism for chemical differentiation, crustal assimilation and the formation of evolved magmas. *J. Petrol.* **53**, 1999–2026 (2012).
97. Boudier, F., Nicolas, A. & Ildefonse, B. Magma chambers in the Oman ophiolite: fed from the top and the bottom. *Earth Planet. Sci. Lett.* **144**, 239–250 (1996).
98. Carbotte, S. M. et al. Stacked sills forming a deep melt-mush feeder conduit beneath Axial Seamount. *Geology* **48**, 693–697 (2020).
99. Bachmann, O. & Bergantz, G. W. Rhyolites and their source mushes across tectonic settings. *J. Petrol.* **49**, 2277–2285 (2008).
100. Spiegelman, M., Kelemen, P. B. & Aharonov, E. Causes and consequences of flow organization during melt transport: the reaction infiltration instability in compactible media. *J. Geophys. Res. Solid Earth* **106**, 2061–2077 (2001).
101. Lissenberg, C. J. & MacLeod, C. J. A reactive porous flow control on mid-ocean ridge magmatic evolution. *J. Petrol.* **57**, 2195–2220 (2016).
102. Bouilhol, P., Schmidt, M. & Burg, J.-P. Magma transfer and evolution in channels within the arc crust: the pyroxenitic feeder pipes of Sapat (Kohistan, Pakistan). *J. Petrol.* **56**, 1309–1342 (2015).
103. Sanfilippo, A., MacLeod, C. J., Tribuzio, R., Lissenberg, C. J. & Zanetti, A. Early-stage melt-rock reaction in a cooling crystal mush beneath a slow-spreading mid-ocean ridge (IODP Hole U1473A, Atlantis Bank, Southwest Indian Ridge). *Front. Earth Sci.* **8**, 579138 (2020).
104. Chadam, J., Hoff, D., Merino, E., Ortoleva, P. & Sen, A. Reactive infiltration instabilities. *IMA J. Appl. Math.* **36**, 207–221 (1986).
105. Spiegelman, M. Flow in deformable porous media. Part 1 simple analysis. *J. Fluid Mech.* **247**, 17–38 (1993).
106. Ryan, A. G., Hansen, L. N., Zimmerman, M. E. & Pistone, M. Melt migration in crystal mushes by viscous fingering: insights from high-temperature, high-pressure experiments. *JGR Solid Earth* **127**, e2022JB024447 (2022).
107. Richter, F. M. & McKenzie, D. Dynamical models for melt segregation from a deformable matrix. *J. Geol.* **92**, 729–740 (1984).
108. Seropian, G., Rust, A. & Sparks, R. The gravitational stability of lenses in magma mushes: confined Rayleigh–Taylor instabilities. *J. Geophys. Res. Solid Earth* **123**, 3593–3607 (2018).
109. Connolly, J. & Podladchikov, Y. Y. Decompaction weakening and channeling instability in ductile porous media: Implications for asthenospheric melt segregation. *J. Geophys. Res. Solid Earth* https://doi.org/10.1029/2005JB004213 (2007).
110. Riel, N. et al. Interaction between mantle-derived magma and lower arc crust: quantitative reactive melt flow modelling using STyx. *Geol. Soc. Spec. Publ.* **478**, 65–87 (2019).
111. Petford, N., Koenders, M. & Clemens, J. D. Igneous differentiation by deformation. *Contrib. Mineral. Petrol.* **175**, 45 (2020).
112. Carrara, A., Burgisser, A. & Bergantz, G. W. Lubrication effects on magmatic mush dynamics. *J. Volcanol. Geotherm. Res.* **380**, 19–30 (2019).
113. Van der Molen, I. & Paterson, M. Experimental deformation of partially-melted granite. *Contrib. Mineral. Petrol.* **70**, 299–318 (1979).
114. Ryan, A. G. et al. Shear-induced dilation and dike formation during mush deformation. *Earth Planet. Sci. Lett.* **651**, 119164 (2025).
115. Rosenberg, C. L. & Handy, M. R. Experimental deformation of partially melted granite revisited: implications for the continental crust. *J. Metamorph. Geol.* **23**, 19–28 (2005).
116. Rummel, L., Kaus, B. J., Baumann, T. S., White, R. W. & Riel, N. Insights into the compositional evolution of crustal magmatic systems from coupled petrological–geodynamical models. *J. Petrol.* **61**, egaa029 (2020).
117. Liu, B. & Lee, C.-T. Fast melt expulsion from crystal-rich mushes via induced anisotropic permeability. *Earth Planet. Sci. Lett.* **571**, 117113 (2021).
118. Allan, A. S., Morgan, D. J., Wilson, C. J. & Millet, M.-A. From mush to eruption in centuries: assembly of the super-sized Oruanui magma body. *Contrib. Mineral. Petrol.* **166**, 143–164 (2013).
119. Cembrano, J. & Lara, L. The link between volcanism and tectonics in the southern volcanic zone of the Chilean Andes: a review. *Tectonophysics* **471**, 96–113 (2009).
120. Humphreys, M. & Holness, M. Melt-rich segregations in the Skaergaard Marginal Border Series: tearing of a vertical silicate mush. *Lithos* **119**, 181–192 (2010).
121. Namur, O., Humphreys, M. C. & Holness, M. B. Lateral reactive infiltration in a vertical gabbroic crystal mush, Skaergaard intrusion, East Greenland. *J. Petrol.* **54**, 985–1016 (2013).
122. Li, J.-Y., Wang, X.-L., Gu, Z.-D., Wang, D. & Du, D.-H. Geochemical diversity of continental arc basaltic mushy reservoirs driven by reactive melt infiltration. *Commun. Earth Environ.* **5**, 109 (2024).
123. Boulanger, M. & France, L. Cumulate formation and melt extraction from mush-dominated magma reservoirs: the melt flush process exemplified at mid-ocean ridges. *J. Petrol.* **64**, egad005 (2023).
124. Leuthold, J. et al. Partial melting of lower oceanic crust gabbro: constraints from poikilitic clinopyroxene primocrysts. *Front. Earth Sci.* **6**, 15 (2018).
125. Huber, C., Bachmann, O. & Dufek, J. Thermo-mechanical reactivation of locked crystal mushes: melting-induced internal fracturing and assimilation processes in magmas. *Earth Planet. Sci. Lett.* **304**, 443–454 (2011).
126. Hepworth, L. N., O'Driscoll, B., Gertisser, R., Daly, J. S. & Emeleus, C. H. Linking in situ crystallization and magma replenishment via sill intrusion in the Rum Western Layered Intrusion, NW Scotland. *J. Petrol.* **59**, 1605–1642 (2018).
127. Hu, H., Jackson, M. D. & Blundy, J. Melting, compaction and reactive flow: controls on melt fraction and composition change in crustal mush reservoirs. *J. Petrol.* **63**, egac097 (2022).
128. Kohlstedt, D. L. & Holtzman, B. K. Shearing melt out of the Earth: an experimentalist's perspective on the influence of deformation on melt extraction. *Annu. Rev. Earth Planet. Sci.* **37**, 561–593 (2009).
129. Smith, D. J. Clinopyroxene precursors to amphibole sponge in arc crust. *Nat. Commun.* **5**, 4329 (2014).
130. Lissenberg, C. J., MacLeod, C. J., Howard, K. A. & Godard, M. Pervasive reactive melt migration through fast-spreading lower oceanic crust (Hess Deep, equatorial Pacific Ocean). *Earth Planet. Sci. Lett.* **361**, 436–447 (2013).
131. Zhang, W.-Q. & Liu, C.-Z. Crust-scale reactive porous flow revealed by the brown amphibole in the IODP Hole U1473A gabbros, Southwest Indian Ridge. *Lithos* **450**, 107209 (2023).
132. Gleeson, M. L., Lissenberg, C. J. & Antoshechkina, P. M. Porosity evolution of mafic crystal mush during reactive flow. *Nat. Commun.* **14**, 3088 (2023).
133. Yang, A. Y., Wang, C., Liang, Y. & Lissenberg, C. J. Reaction between mid-ocean ridge basalt and lower oceanic crust: an experimental study. *Geochem. Geophys. Geosyst.* **20**, 4390–4407 (2019).
134. Blundy, J. Chemical differentiation by mineralogical buffering in crustal hot zones. *J. Petrol.* **63**, egac054 (2022).
135. Müntener, O. & Ulmer, P. Arc crust formation and differentiation constrained by experimental petrology. *Am. J. Sci.* **318**, 64–89 (2018).
136. Blatter, D. L., Sisson, T. W. & Hankins, W. B. Voluminous arc dacites as amphibole reaction-boundary liquids. *Contrib. Mineral. Petrol.* **172**, 1–37 (2017).
137. Ulmer, P., Kaegi, R. & Müntener, O. Experimentally derived intermediate to silica-rich arc magmas by fractional and equilibrium crystallization at 1·0 GPa: an evaluation of phase relationships, compositions, liquid lines of descent and oxygen fugacity. *J. Petrol.* **59**, 11–58 (2018).
138. Hepworth, L. N. et al. Rapid crystallization of precious-metal-mineralized layers in mafic magmatic systems. *Nat. Geosci.* **13**, 375–381 (2020).
139. Lissenberg, C. J. & Dick, H. J. Melt–rock reaction in the lower oceanic crust and its implications for the genesis of mid-ocean ridge basalt. *Earth Planet. Sci. Lett.* **271**, 311–325 (2008).

140. Gudmundsson, A. The mechanics of large volcanic eruptions. *Earth Sci. Rev.* **163**, 72–93 (2016).
141. Cooper, K. M. Time scales and temperatures of crystal storage in magma reservoirs: implications for magma reservoir dynamics. *Philos. Trans. R. Soc. A* **377**, 20180009 (2019).
142. Cooper, K. M. & Kent, A. J. Rapid remobilization of magmatic crystals kept in cold storage. *Nature* **506**, 480–483 (2014).
143. Molina, P. G. et al. Protracted late magmatic stage of the Caleu pluton (central Chile) as a consequence of heat redistribution by diking: Insights from zircon data and thermal modeling. *Lithos* **227**, 255–268 (2015).
144. Bachmann, O., Dungan, M. A. & Lipman, P. W. The Fish Canyon magma body, San Juan volcanic field, Colorado: rejuvenation and eruption of an upper-crustal batholith. *J. Petrol.* **43**, 1469–1503 (2002).
145. Spera, F. J. & Bohrson, W. A. Rejuvenation of crustal magma mush: a tale of multiply nested processes and timescales. *Am. J. Sci.* **318**, 90–140 (2018).
146. Huber, C., Bachmann, O. & Manga, M. Two competing effects of volatiles on heat transfer in crystal-rich magmas: thermal insulation vs defrosting. *J. Petrol.* **51**, 847–867 (2010).
147. Huber, C., Bachmann, O. & Dufek, J. The limitations of melting on the reactivation of silicic mushes. *J. Volcanol. Geotherm. Res.* **195**, 97–105 (2010).
148. Passmore, E., Maclennan, J., Fitton, G. & Thordarson, T. Mush disaggregation in basaltic magma chambers: evidence from the AD 1783 Laki eruption. *J. Petrol.* **53**, 2593–2623 (2012).
149. Moore, A., Coogan, L., Costa, F. & Perfit, M. Primitive melt replenishment and crystal-mush disaggregation in the weeks preceding the 2005–2006 eruption 9 50′ N, EPR. *Earth Planet. Sci. Lett.* **403**, 15–26 (2014).
150. Christopher, T. E. et al. Crustal-scale degassing due to magma system destabilization and magma-gas decoupling at Soufriere Hills Volcano, Montserrat. *Geochem. Geophys. Geosyst.* **16**, 2797–2811 (2015).
151. Carrara, A. & Bergantz, G. W. Numerical simulations of the mingling caused by a magma intruding a resident mush. *Volcanica* **7**, 89–104 (2024).
152. Bachmann, O. & Bergantz, G. W. Gas percolation in upper-crustal silicic crystal mushes as a mechanism for upward heat advection and rejuvenation of near-solidus magma bodies. *J. Volcanol. Geotherm. Res.* **149**, 85–102 (2006).
153. Connolly, J. A. D. & Podladchikov, Y. Y. in *Metasomatism and the Chemical Transformation of Rock* (eds Harlov, D. E. & Austrheim, H.) 599–658 (Springer, 2013); https://doi.org/10.1007/978-3-642-28394-9_14.
154. Spera, F. J. & Bohrson, W. A. Energy-constrained open-system magmatic processes I: general model and energy-constrained assimilation and fractional crystallization (EC-AFC) formulation. *J. Petrol.* **42**, 999–1018 (2001).
155. Burgisser, A. & Bergantz, G. W. A rapid mechanism to remobilize and homogenize highly crystalline magma bodies. *Nature* **471**, 212–215 (2011).
156. Hickey-Vargas, R., Abdollahi, M. J., Parada, M. A., López-Escobar, L. & Frey, F. A. Crustal xenoliths from Calbuco Volcano, Andean Southern Volcanic Zone: implications for crustal composition and magma–crust interaction. *Contrib. Mineral. Petrol.* **119**, 331–344 (1995).
157. Costa, F., Dungan, M. A. & Singer, B. S. Hornblende- and phlogopite-bearing gabbroic xenoliths from Volcán San Pedro (36°S), Chilean Andes: evidence for melt and fluid migration and reactions in subduction-related plutons. *J. Petrol.* **43**, 219–241 (2002).
158. Clemens, J., Stevens, G., Frei, D. & Joseph, C. Origins of cryptic variation in the ediacaran–fortunian rhyolitic ignimbrites of the Saldanha Bay Volcanic Complex, Western Cape, South Africa. *Contrib. Mineral. Petrol.* **172**, 1–23 (2017).
159. Humphreys, M. C. et al. Unravelling the complexity of magma plumbing at Mount St. Helens: a new trace element partitioning scheme for amphibole. *Contrib. Mineral. Petrol.* **174**, 1–15 (2019).
160. Hughes, G. E., Petrone, C. M., Downes, H., Varley, N. R. & Hammond, S. J. Mush remobilisation and mafic recharge: a study of the crystal cargo of the 2013–17 eruption at Volcán de Colima, Mexico. *J. Volcanol. Geotherm. Res.* **416**, 107296 (2021).
161. Klaver, M., Blundy, J. D. & Vroon, P. Z. Generation of arc rhyodacites through cumulate–melt reactions in a deep crustal hot zone: evidence from Nisyros volcano. *Earth Planet. Sci. Lett.* **497**, 169–180 (2018).
162. Erdmann, S., Scaillet, B. & Kellett, D. Textures of peritectic crystals as guides to reactive minerals in magmatic systems: new insights from melting experiments. *J. Petrol.* **53**, 2231–2258 (2012).
163. Watts, K. E., Bindeman, I. N. & Schmitt, A. K. Crystal scale anatomy of a dying supervolcano: an isotope and geochronology study of individual phenocrysts from voluminous rhyolites of the Yellowstone caldera. *Contrib. Mineral. Petrol.* **164**, 45–67 (2012).
164. Claiborne, L. L. et al. Tracking magmatic processes through Zr/Hf ratios in rocks and Hf and Ti zoning in zircons: an example from the Spirit Mountain batholith, Nevada. *Mineral. Mag.* **70**, 517–543 (2006).
165. Cooper, K. M. Timescales of crustal magma reservoir processes: insights from U-series crystal ages. *Geol. Soc. Spec. Publ.* **422**, 141–174 (2015).
166. Andersen, N. L., Jicha, B. R., Singer, B. S. & Hildreth, W. Incremental heating of Bishop Tuff sanidine reveals preeruptive radiogenic Ar and rapid remobilization from cold storage. *Proc. Natl Acad. Sci. USA* **114**, 12407–12412 (2017).
167. Cooper, G. F., Morgan, D. J. & Wilson, C. J. Rapid assembly and rejuvenation of a large silicic magmatic system: insights from mineral diffusive profiles in the Kidnappers and Rocky Hill deposits, New Zealand. *Earth Planet. Sci. Lett.* **473**, 1–13 (2017).
168. Jollands, M. C., Bloch, E. & Müntener, O. New Ti-in-quartz diffusivities reconcile natural Ti zoning with time scales and temperatures of upper crustal magma reservoirs. *Geology* **48**, 654–657 (2020).
169. Chamberlain, K. J., Morgan, D. J. & Wilson, C. J. N. Timescales of mixing and mobilisation in the Bishop Tuff magma body: perspectives from diffusion chronometry. *Contrib. Mineral. Petrol.* **168**, 1034 (2014).
170. Weber, G., Blundy, J. & Bevan, D. Mush amalgamation, short residence, and sparse detectability of eruptible magma before andean super-eruptions. *Geochem. Geophys. Geosyst.* **24**, e2022GC010732 (2023).
171. Grocolas, T., Bloch, E. M., Bouvier, A.-S. & Müntener, O. Diffusion of Sr and Ba in plagioclase: composition and silica activity dependencies, and application to volcanic rocks. *Earth Planet. Sci. Lett.* **651**, 119141 (2025).
172. Costa, F., Andreastuti, S., de Maisonneuve, C. B. & Pallister, J. S. Petrological insights into the storage conditions, and magmatic processes that yielded the centennial 2010 Merapi explosive eruption. *J. Volcanol. Geotherm. Res.* **261**, 209–235 (2013).
173. Morgado, E. et al. Old magma and a new, intrusive trigger: using diffusion chronometry to understand the rapid-onset Calbuco eruption, April 2015 (Southern Chile). *Contrib. Mineral. Petrol.* **174**, 1–11 (2019).
174. Barboni, M. et al. Warm storage for arc magmas. *Proc. Natl. Acad. Sci. USA.* **113**, 13959–13964 (2016).
175. Cooper, G. F., Wilson, C. J., Millet, M.-A., Baker, J. A. & Smith, E. G. Systematic tapping of independent magma chambers during the 1 Ma Kidnappers supereruption. *Earth Planet. Sci. Lett.* **313**, 23–33 (2012).
176. Mallea-Lillo, F., Parada, M. A., Morgado, E., Contreras, C. & Hübner, D. Contrasting sources and conditions of shallow magmatic reservoirs of the Fui Group small eruptive centres associated with the Liquiñe-Ofqui Fault Zone (Chilean Andes). *J. South Am. Earth Sci.* **117**, 103875 (2022).
177. Huber, C., Bachmann, O. & Manga, M. Homogenization processes in silicic magma chambers by stirring and mushification (latent heat buffering). *Earth Planet. Sci. Lett.* **283**, 38–47 (2009).
178. Booth, C. A., Jackson, M. D., Sparks, R. S. J. & Rust, A. C. Source reservoir controls on the size, frequency, and composition of large-scale volcanic eruptions. *Sci. Adv.* **10**, eadd1595 (2024).
179. Spera, F. Thermal evolution of plutons: a parameterized approach. *Science* **207**, 299–301 (1980).
180. Farner, M. J. & Lee, C.-T. A. Effects of crustal thickness on magmatic differentiation in subduction zone volcanism: a global study. *Earth Planet. Sci. Lett.* **470**, 96–107 (2017).
181. Bea, F. The sources of energy for crustal melting and the geochemistry of heat-producing elements. *Lithos* **153**, 278–291 (2012).
182. Schaen, A. J. et al. Transient rhyolite melt extraction to produce a shallow granitic pluton. *Sci. Adv.* **7**, eabf0604 (2021).
183. Walker, B. A., Grunder, A. L. & Wooden, J. L. Organization and thermal maturation of long-lived arc systems: evidence from zircons at the Aucanquilcha Volcanic Cluster, northern Chile. *Geology* **38**, 1007–1010 (2010).
184. Grunder, A. L., Klemetti, E. W., Feeley, T. C. & McKee, C. M. Eleven million years of arc volcanism at the Aucanquilcha Volcanic Cluster, northern Chilean Andes: implications for the life span and emplacement of plutons. *Trans. Roy. Soc. Edinb. Earth Sci.* **97**, 415–436 (2008).
185. Dufek, J. & Bergantz, G. Lower crustal magma genesis and preservation: a stochastic framework for the evaluation of basalt–crust interaction. *J. Petrol.* **46**, 2167–2195 (2005).
186. Hawkesworth, C. et al. Time scales of crystal fractionation in magma chambers — integrating physical, isotopic and geochemical perspectives. *J. Petrol.* **41**, 991–1006 (2000).
187. Lissenberg, C. J., Rioux, M., Shimizu, N., Bowring, S. A. & Mével, C. Zircon dating of oceanic crustal accretion. *Science* **323**, 1048–1050 (2009).
188. Laporte, D., Rapaille, C. & Provost, A. in *Granite: from Segregation of Melt to Emplacement Fabrics* (eds Laporte, D. et al.) 31–54 (Springer, 1997).
189. Walker, B. A. Jr, Bergantz, G. W., Otamendi, J. E., Ducea, M. N. & Cristofolini, E. A. A MASH zone revealed: the mafic complex of the Sierra Valle Fértil. *J. Petrol.* **56**, 1863–1896 (2015).
190. Schaltegger, U. et al. Zircon petrochronology and $^{40}Ar/^{39}Ar$ thermochronology of the Adamello Intrusive Suite, N. Italy: monitoring the growth and decay of an incrementally assembled magmatic system. *J. Petrol.* **60**, 701–722 (2019).
191. Morgan, C., Morgado, E., Parada, M.-Á., Brahm, R. & Mallea-Lillo, F. Two-stage evolution of a bimodal reservoir: the case of Holocene lavas of the Lanín composite volcano, Southern Volcanic Zone, Chile. *J. South Am. Earth Sci.* **133**, 104697 (2024).
192. Gutiérrez, F. & Parada, M. A. Numerical modeling of time-dependent fluid dynamics and differentiation of a shallow basaltic magma chamber. *J. Petrol.* **51**, 731–762 (2010).
193. Wark, D., Kempter, K. & McDowell, F. Evolution of waning, subduction-related magmatism, northern Sierra Madre Occidental, Mexico. *Geol. Soc. Am. Bull.* **102**, 1555–1564 (1990).
194. Godoy, B. et al. Linking the mafic volcanism with the magmatic stages during the last 1 Ma in the main volcanic arc of the Altiplano-Puna Volcanic Complex (Central Andes). *J. South Am. Earth Sci.* **95**, 102295 (2019).
195. Moore, N. E., Grunder, A. L., Bohrson, W. A., Carlson, R. W. & Bindeman, I. N. Changing mantle sources and the effects of crustal passage on the steens basalt, SE Oregon: chemical and isotopic constraints. *Geochem. Geophys. Geosyst.* **21**, e2020GC008910 (2020).

196. Broderick, C. et al. Linking the thermal evolution and emplacement history of an upper-crustal pluton to its lower-crustal roots using zircon geochronology and geochemistry (southern Adamello batholith, N. Italy). *Contrib. Mineral. Petrol.* **170**, 28 (2015).
197. Loucks, R. R. Deep entrapment of buoyant magmas by orogenic tectonic stress: its role in producing continental crust, adakites, and porphyry copper deposits. *Earth Sci. Rev.* **220**, 103744 (2021).
198. Hartung, E., Weber, G. & Caricchi, L. The role of H_2O on the extraction of melt from crystallising magmas. *Earth Planet. Sci. Lett.* **508**, 85–96 (2019).
199. Boulanger, M. et al. Magma reservoir formation and evolution at a slow-spreading center (Atlantis Bank, Southwest Indian Ridge). *Front. Earth Sci.* **8**, 554598 (2020).
200. Riel, N., Kaus, B. J. P., Green, E. C. R. & Berlie, N. MAGEMin, an efficient gibbs energy minimizer: application to igneous systems. *Geochem. Geophys. Geosyst.* **23**, e2022GC010427 (2022).
201. Holland, T. J. B., Green, E. C. R. & Powell, R. Melting of peridotites through to granites: a simple thermodynamic model in the system KNCFMASHTOCr. *J. Petrol.* **59**, 881–900 (2018).
202. Grove, T. L. & Kinzler, R. J. Petrogenesis of andesites. *Annu. Rev. Earth Planet. Sci.* **14**, 417–454 (1986).
203. Gale, A., Dalton, C. A., Langmuir, C. H., Su, Y. & Schilling, J. The mean composition of ocean ridge basalts. *Geochem. Geophys. Geosyst.* **14**, 489–518 (2013).
204. Plank, T. & Langmuir, C. H. An evaluation of the global variations in the major element chemistry of arc basalts. *Earth Planet. Sci. Lett.* **90**, 349–370 (1988).
205. Villiger, S., Ulmer, P. & Muntener, O. Equilibrium and fractional crystallization experiments at 0·7 GPa; the effect of pressure on phase relations and liquid compositions of tholeiitic magmas. *J. Petrol.* **48**, 159–184 (2006).
206. Villiger, S. The liquid line of descent of anhydrous, mantle-derived, tholeiitic liquids by fractional and equilibrium crystallization-an experimental study at 1·0 GPa. *J. Petrol.* **45**, 2369–2388 (2004).
207. Nandedkar, R. H., Ulmer, P. & Müntener, O. Fractional crystallization of primitive, hydrous arc magmas: an experimental study at 0.7 GPa. *Contrib. Mineral. Petrol.* **167**, 1015 (2014).
208. Jerram, D. A., Cheadle, M. J. & Philpotts, A. R. Quantifying the building blocks of igneous rocks: are clustered crystal frameworks the foundation? *J. Petrol.* **44**, 2033–2051 (2003).
209. Philpotts, A. R., Shi, J. & Brustman, C. Role of plagioclase crystal chains in the differentiation of partly crystallized basaltic magma. *Nature* **395**, 343–346 (1998).
210. Rudge, J. F., Holness, M. B. & Smith, G. C. Quantitative textural analysis of packings of elongate crystals. *Contrib. Mineral. Petrol.* **156**, 413–429 (2008).
211. Saar, M. O., Manga, M., Cashman, K. V. & Fremouw, S. Numerical models of the onset of yield strength in crystal–melt suspensions. *Earth Planet. Sci. Lett.* **187**, 367–379 (2001).
212. Nolan, G. & Kavanagh, P. Computer simulation of random packings of spheres with log-normal distributions. *Powder Technol.* **76**, 309–316 (1993).
213. He, D., Ekere, N. N. & Cai, L. Computer simulation of random packing of unequal particles. *Phys. Rev. E* **60**, 7098 (1999).
214. Nield, D. A. & Bejan, A. *Convection in Porous Media* Vol. 3 (Springer, 2006).
215. Zakirov, T. R. & Khramchenkov, M. G. Prediction of permeability and tortuosity in heterogeneous porous media using a disorder parameter. *Chem. Eng. Sci.* **227**, 115893 (2020).
216. Hersum, T. Consequences of crystal shape and fabric on anisotropic permeability in magmatic mush. *Contrib. Mineral. Petrol.* **157**, 285–300 (2009).
217. Vasseur, J., Wadsworth, F. B., Coumans, J. P. & Dingwell, D. B. Permeability of packs of polydisperse hard spheres. *Phys. Rev. E* **103**, 062613 (2021).
218. Bretagne, E., Wadsworth, F. B., Vasseur, J. & Dobson, K. J. A scaling for the permeability of loose magma mush validated using X-ray computed tomography of packed confectionary in 3D and estimation methods from 2D crystal shapes. *J. Geophys. Res. Solid Earth* **128**, e2023JB026795 (2023).
219. Vasseur, J., Wadsworth, F. B., Bretagne, E. & Dingwell, D. B. Universal scaling for the permeability of random packs of overlapping and nonoverlapping particles. *Phys. Rev. E* **105**, L043301 (2022).
220. Röding, M., Ma, Z. & Torquato, S. Predicting permeability via statistical learning on higher-order microstructural information. *Sci. Rep.* **10**, 1–17 (2020).
221. Rosenberg, N. & Spera, F. Role of anisotropic and/or layered permeability in hydrothermal convection. *Geophys. Res. Lett.* **17**, 235–238 (1990).
222. Hunter, R. H. in *Origins of Igneous Layering* (ed. Parsons, I.) 473–503 (Springer, 1987).
223. Holness, M., Clemens, J. & Vernon, R. How deceptive are microstructures in granitic rocks? Answers from integrated physical theory, phase equilibrium, and direct observations. *Contrib. Mineral. Petrol.* **173**, 1–18 (2018).

Acknowledgements

M.C.S.H. has received funding from the European Research Council (ERC) under the European Union's Horizon 2020 research and innovation programme (grant agreement no. 864923), and also acknowledges support from the UK Natural Environment Research Council (grant NE/T000430/1). M.C.S.H. thanks F. Wadsworth, E. Llewellin, M. Holness and members of the mush group at Durham for helpful comments on the manuscript, and C. Annen for useful discussions. O.N. acknowledges support from Fonds Wetenschappelijk Onderzoek for multiple projects. O.N. thanks M. Holness for very useful suggestions. C.H. acknowledges support from NSF EAR-2021328. W.A.B. acknowledges support from the US National Science Foundation. P.B. acknowledges funding from INSU and OTElo and fruitful discussions with L. France. G.F.C. is funded by a Royal Society University Research Fellowship 2022. K.C. acknowledges support from the US National Science Foundation for multiple projects that contributed to the development of these ideas. C.J.L. was supported by the Natural Environment Research Council. F.S. gratefully acknowledges funding by the US National Science Foundation and the US Department of Energy over many years for studies of magmatic systems.

Author contributions

All authors contributed to discussion of the content, and to the writing, reviewing and editing of the manuscript before submission.

Competing interests

The authors declare no competing interests.

Additional information

Peer review information *Nature Reviews Earth & Environment* thanks George Bergantz, Othmar Müntener and the other, anonymous, reviewer for their contribution to the peer review of this work.